

Outer-Loop Control Design and Simulation Handling Qualities Assessment for a Coaxial-Compound Helicopter and Tiltrotor

Tom Berger

Aerospace Engineer
U.S. Army Combat Capabilities Development
Command Aviation & Missile Center
Moffett Field, CA, USA

Mark B. Tischler

Senior Technologist
U.S. Army Combat Capabilities Development
Command Aviation & Missile Center
Moffett Field, CA, USA

Joseph F. Horn

Professor
Department of Aerospace Engineering
The Pennsylvania State University
University Park, PA, USA

ABSTRACT

This paper describes the development of full flight envelope dynamic inversion outer-loop control laws used to control airspeed and flight path for two Future Vertical Lift-relevant rotorcraft configurations—a lift offset coaxial helicopter with a pusher propeller and a tiltrotor. The outer-loop control laws for both aircraft include a control allocation scheme to account for redundant controls and reduce pilot workload. A piloted simulation experiment was conducted at the Penn State Flight Simulator facility using a series of high-speed handling qualities demonstration maneuvers to evaluate the handling qualities of the control laws. Overall, the outer-loop control laws for both coaxial-pusher and tiltrotor aircraft were assigned Level 1 handling qualities for the Break Turn and High-Speed Acceleration/Deceleration tasks, and reduced pilot workload over previously developed inner-loop control laws. The outer-loop control laws also improved performance and reduced pilot workload in a formation flying task developed for this experiment. The coaxial-pusher outer-loop control laws received borderline Level 1/Level 2 ratings for the Pitch Attitude Capture and Hold and Sum-of-Sines Tracking tasks, while the tiltrotor outer-loop control laws (with their increased value of pitch attitude dropback) received Level 2 ratings.

NOTATION

Symbols

δ_{col}	Symmetric main rotor collective [deg]
δ_{nac}	Nacelle tilt angle [deg]
δ_{prop}	Pusher propeller collective [deg]
$\dot{\cdot}$	Derivative with respect to time
γ	Flight path angle [deg]
ω	Natural frequency [rad/sec]
A, B, C, D	State-space representation (standard form)
M	Control allocation matrix
u	Input vector
x	State vector
y	Output vector

τ	Time constant or time delay [sec]
θ	Pitch attitude [deg]
ζ	Damping ratio [-]
g	Acceleration due to gravity [ft/sec ²]
h	Altitude [ft]
K	Gain
n_z	Normal acceleration [g]
P	Power [hp or ft-lb/sec]
T_{θ_2}	Flight path-attitude lag [sec]
V	Airspeed [kts]
W	Weight [lb]

Subscripts

0	Trim
BW	Bandwidth
CAS	Calibrated airspeed
cm	Commanded response
col	Collective
lon	Longitudinal
OL	Outer loop

Presented at the VFS International 76th Annual Forum & Technology Display, Virginia Beach, Virginia, October 6–8, 2020. This is work of the U.S. Government and is not subject to copyright protection in the U.S. Distribution Statement A. Approved for public release; distribution is unlimited.

s Pilot stick input
TAS True airspeed

Acronyms

BWLR Bedford Workload Rating
HQR Cooper-Harper Handling Qualities Rating
KCAS Knots Calibrated Airspeed
KTAS Knots True Airspeed
PIO Pilot Induced Oscillation

INTRODUCTION

With the development of advanced high-speed rotorcraft, through the U.S. Army Future Vertical Lift (FVL) modernization priority, new high-speed handling qualities requirements are needed to ensure safe and low-workload piloting in the transition and high-speed regimes. The Combat Capability Development Command (CCDC) Aviation & Missile Center (AvMC) Technology Development Directorate (TDD) has developed high-fidelity flight-dynamics models of generic FVL configurations to provide the government with independent control-system design, handling-qualities analysis, and simulation research capabilities for advanced high-speed rotorcraft. Two of these generic models are a lift offset coaxial helicopter with compound thrust provided through a pusher propeller (herein referred to as *coaxial-pusher*) and *tiltrotor* aircraft. The two aircraft fall under the FVL Capabilities Set #3 (Ref. 1), or Future Long Range Assault Aircraft (FLRAA) category. The models were developed using the comprehensive rotorcraft simulation code HeliUM (Refs. 2, 3), and are described in detail in Ref. 4. The models are generic in nature and not meant to represent specific aircraft (such as the SB>1 or V-280). A rendering of the models is shown in Figure 1.

A set of full flight envelope *inner-loop* (Rate-Command/Attitude-Hold, RCAH) control laws were previously designed and tested in piloted simulation for both aircraft (Ref. 5). The piloted simulation was conducted in the NASA Ames Vertical Motion Simulator (VMS) facility using five Army experimental test pilots (XPs). A set of high-speed handling-qualities demonstration maneuvers (or Mission Task Elements, MTEs) developed by the National Rotorcraft Technology Center (NRTC) and flight tested by TDD (Ref. 6) were used in the evaluation: Pitch and Bank Attitude Capture and Hold (Ref. 7), Pitch and Roll Sum-of-Sines Tracking (Ref. 8), Break Turn (Ref. 9) and High-Speed Acceleration/Deceleration (Ref. 10). Overall, both aircraft received Level 1 handling qualities ratings by the pilots, however it was apparent that *outer-loop* (airspeed and flight path/climb rate) control laws would improve the handling qualities and reduce pilot workload, especially for the Break Turn and High-Speed Acceleration/Deceleration MTEs. This is especially true

for the advanced configurations considered here, since they both have a redundant control that the pilot must use to regulate airspeed and climb rate in addition to the typical pitch attitude and main rotor collective control. In the case of the coaxial-pusher, the pilot must also control the pusher propeller collective, while in the case of the tiltrotor, the pilot must manage the nacelle tilt angle.

This paper describes the development and testing of the outer-loop control laws for both coaxial-pusher and tiltrotor aircraft. A dynamic inversion (DI) architecture was used for the outer-loop control laws, with a control allocation scheme for each aircraft to account for the outer-loop redundant control. The Control Designer's Unified Interface (CONDUIT[®]) and design methods of Ref. 11 were used to optimize the outer-loop control laws to meet a wide range of stability, handling-qualities, and performance specifications throughout the aircraft flight envelopes. The coaxial-pusher design met the Level 1 requirement for all specifications. In the case of the tiltrotor, with its larger value of flight path-attitude lag, there was a trade-off between the flight path bandwidth and pitch attitude dropback requirements, and both could not be met simultaneously for part of the flight envelope. The larger flight path-attitude lag value for the tiltrotor model is consistent with other tiltrotor designs (e.g., Ref. 12).

A piloted simulation assessment of the outer-loop control law handling qualities was conducted in the Pennsylvania State University (PSU) Flight Simulator facility using two Army XPs. A subset of the NRTC high-speed MTEs used to investigate the inner-loop control laws were used, in addition to a formation flying task developed for this experiment. Overall, the outer-loop control laws for both coaxial-pusher and tiltrotor aircraft were assigned Level 1 handling qualities for the Break Turn and High-Speed Acceleration/Deceleration tasks, and reduced pilot workload over previously developed inner-loop control laws. The outer-loop control laws also improved performance and reduced pilot workload in a formation flying task developed for this experiment. The coaxial-pusher outer loops received borderline Level 1/Level 2 ratings for the Pitch Attitude Capture and Hold and Sum-of-Sines Tracking tasks, while the tiltrotor outer loops (with their increased value of pitch attitude dropback) received Level 2 ratings.

The remainder of this paper provides a brief overview of the coaxial-pusher and tiltrotor models. Following that, a description of the flight control systems for both aircraft is given, including the architecture, design specifications, and optimization results. After a brief description of the simulation experimental setup, the results of the experiment are provided first for the coaxial-pusher and then for the tiltrotor. This will be followed by a discussion of the results and conclusions.

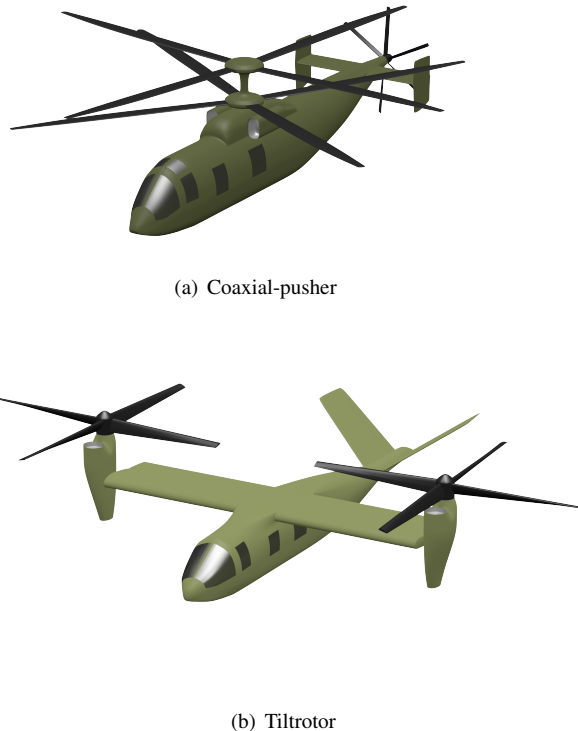


Fig. 1. Generic aircraft schematics.

VEHICLE MODELS

The flight-dynamics models of the lift offset coaxial-pusher and tiltrotor configurations were developed using HeliUM-A, the CCDC AvMC TDD in-house flight-dynamics modeling software tool developed as an extension to the University of Maryland HeliUM simulation model (Refs. 2, 3). HeliUM-A uses a finite-element approach to model flexible rotor blades with coupled nonlinear flap/lag/torsion dynamics to capture structural, inertial, and aerodynamic loads along each blade segment, a key requirement for these advanced rotorcraft configurations. Blade, wing, and fuselage aerodynamics come from nonlinear lookup tables, and the rotor airwakes are modeled using a dynamic inflow model. A multi-body like modeling approach is used to build the aircraft configuration from its independent components (e.g., fuselage, wing, nacelle, etc.), which allows modeling of arbitrary aircraft configuration with multiple rotors.

The models are generic and are not meant to represent specific industry designs. Both aircraft have gross weights of roughly 32,000 lbs and fall into the FVL Capabilities Set #3, or Future Long Range Assault Aircraft (FLRAA) category. The flight dynamics of both aircraft are modeled from hover to $V = 300$ kts, however, the maximum airspeeds of the models are limited to $V_H = 240$ kts for the coaxial-pusher and $V_H = 280$ kts for the tiltrotor using notional engine models.

The coaxial-pusher configuration was derived from a previous rotorcraft sizing trade-off study (Ref. 13), which gives the overall dimensional and weight characteristics as well as key rotor and aircraft aerodynamic properties. The generic tiltrotor configuration was derived from scaling geometric, inertial, and structural properties of the XV-15, V-22, and the notional NASA Large Civil Tilt-Rotor 2 (LCTR2). Berger et al. (Ref. 4) presents a detailed description of the coaxial-pusher and tiltrotor models.

Linear state-space point models and trim data were extracted from HeliUM-A at a range of airspeeds and altitudes. The linear models contain the rigid body states, the first two blade modes for each rotor (modeled as one collective, two cyclic, and one reactionless second-order rotor states), three (average, cosine, and sine) inflow states per rotor, as well as a pusher propeller inflow state for the coaxial-pusher and second-order nacelle angle dynamics for the tiltrotor. Overall the coaxial-pusher linear models contain 48 states and the tiltrotor linear models contain 51 states.

The linear point models were used to develop the flight control systems. Furthermore, the point models and trim data were combined to form continuous full-flight envelope quasi-linear parameter varying (qLPV) stitched simulation models (Ref. 14). These models were suitable for real-time simulation, and they formed the basis of the simulation models used in the experiment described here.

FLIGHT CONTROL SYSTEMS

There are three controls that the pilot has to regulate airspeed V and climb rate \dot{h} for both aircraft configurations with the inner-loop control laws (previously designed and described in Ref. 5) closed around the bare-airframe:

1. Pitch attitude θ (governed by the inner-loop control system pitch axis)
2. Symmetric main rotor collective δ_{col}
3. Pusher propeller collective δ_{prop} (coaxial-pusher) or nacelle tilt angle δ_{nac} (tiltrotor)

How each of these controls affects airspeed and climb rate is a function of flight condition and aircraft configuration/orientation. During manual control of the closed inner-loop system, the pilot must control the two states with the three available controls, which was seen to increase workload in the VMS handling qualities simulation experiment described in Ref. 5. Therefore, outer-loop control laws were designed for both coaxial-pusher and tiltrotor to control airspeed and climb rate. The outer-loop control laws are based on a dynamic inversion (DI) architecture (Refs. 11, 15) with a top level representation

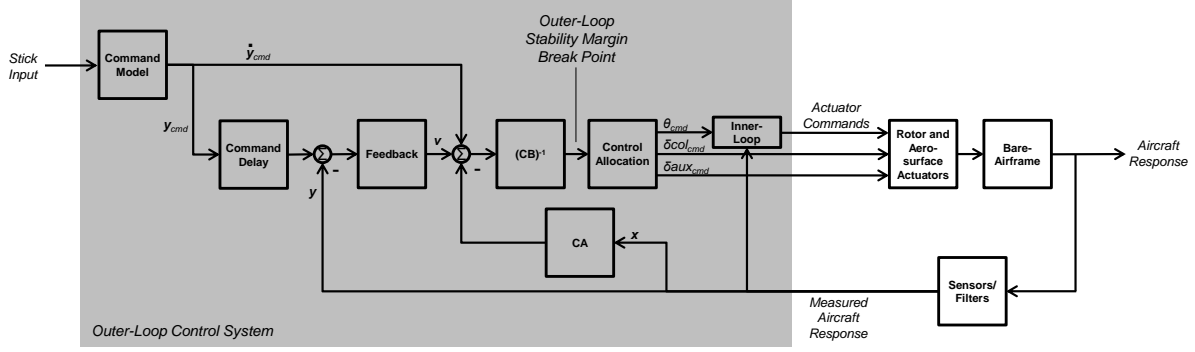


Fig. 2. Top level block diagram representation of outer-loop control system.

shown in Figure 2. The control system consists of six main elements described in more detail in the following sections:

1. Inner-Loop Control System
2. Dynamic Inversion [CA and $(CB)^{-1}$ blocks]
3. Control Allocation
4. Command Model
5. Command Delay
6. Feedback

1. Inner-Loop Control System

The inner-loop control system is based on that presented in Ref. 5, with several modifications made to the pitch axis for integration with the outer-loop control laws. Between hover and $V = 200$ kts, the previously designed inner-loop control laws used a Rate-Command/Attitude-Hold (RCAH) response type in pitch. To accept the outer-loop control law attitude command θ_{cmOL} , the inner-loop pitch response type was changed to Attitude-Command/Attitude-Hold (ACA) by updating the pitch command model.

Above $V = 200$ kts, the previously designed inner-loop control laws used a normal acceleration command response type. Therefore, above $V = 200$ kts, the pitch attitude command generated by the outer-loop control system θ_{cmOL} was converted to a normal acceleration command $n_{z_{cmOL}}$ using the following kinematic relationship (Ref. 16):

$$\frac{n_{z_{cmOL}}}{\theta_{cmOL}} = \frac{(V_{TAS}/g)s}{T_{\theta_2}s + 1} \quad (1)$$

where T_{θ_2} is the flight path-attitude lag, and is taken as equal to $T_{\theta_2} = -1/Z_w$ based on the bare-airframe rigid-body (or quasi-steady) value of Z_w (Ref. 16).

These modifications to the inner-loop control system make the inner loop appear as a pitch attitude actuator to the outer-loop control system. Additional information about these modifications is provided in Ref. 17.

2. Dynamic Inversion

The dynamic inversion (DI) section of the outer-loop control system is comprised of the CA and $(CB)^{-1}$ blocks in Figure 2. These form a feedback loop meant to cancel the plant dynamics (in this case the closed-loop bare-airframe plus inner-loop control system) and make the relationship between the output variables being controlled ($\mathbf{y} = [V \ \dot{h}]^T$) and the inputs (\mathbf{u}) appear as a set of decoupled integrators (Refs. 11, 15, 18).

Since dynamic inversion requires full state feedback, a lower-order (two state, three input) model is used to represent the airspeed V and climb rate \dot{h} dynamics of the bare-airframe *with inner-loop control system closed*:

$$\begin{bmatrix} \dot{V} \\ \dot{h} \end{bmatrix} = \underbrace{\begin{bmatrix} X_V & X_h \\ Z_V & Z_h \end{bmatrix}}_A \begin{bmatrix} V \\ \dot{h} \end{bmatrix} + \underbrace{\begin{bmatrix} X_\theta & X_{\delta_{col}} & X_{\delta_{aux}} \\ Z_\theta & Z_{\delta_{col}} & Z_{\delta_{aux}} \end{bmatrix}}_B \begin{bmatrix} \theta \\ \delta_{col} \\ \delta_{aux} \end{bmatrix} \quad (2)$$

where δ_{aux} represents pusher propeller collective δ_{prop} in the case of the coaxial-pusher and nacelle angle δ_{nac} in the case of the tiltrotor. Since the two states of the system V and \dot{h} are also the outputs to be controlled, $\mathbf{C} = \mathbf{I}$.

The parameters of the lower-order airspeed V and climb rate \dot{h} model given in Eq. 2 can be determined analytically from the bare-airframe model by reducing the bare-airframe to the rigid-body dynamics. This approach was used in Refs. 19 and 20, but ignores the effects of the inner-loop control system. This may be acceptable, since the inner-loop control system operates at higher frequencies than the airspeed V and climb rate \dot{h} dynamics. However, here, system identification was performed on the

closed bare-airframe plus inner-loop system to identify the derivatives in Eq. 2. A frequency domain approach using the CIFER (Ref. 21) tool was used to identify the derivatives across a frequency range of $\omega = 0.001 - 1$ rad/sec. Reference 17 shows a comparison of the analytical approach and system identification approach, and demonstrates the benefits of the latter.

3. Control Allocation

Dynamic inversion requires a square system, however the system representing the closed-loop bare-airframe plus inner-loop control system shown in Eq. 2 has a redundant input. Therefore, a control allocation scheme is required. Different approaches were used for the coaxial-pusher and tiltrotor, which are discussed in the following sections.

Coaxial-Pusher Control Allocation For the coaxial-pusher, a weighted pseudo-inverse method (Refs. 22–24) was used to account for the redundant control (similar to what was done for the inner loop). The control allocation matrix \mathbf{M} is given by:

$$\mathbf{M} = \mathbf{W}^{-1} \mathbf{B}^T (\mathbf{B} \mathbf{W}^{-1} \mathbf{B}^T)^{-1} \quad (3)$$

where \mathbf{B} is the control derivative matrix from Eq. 2 and the weighting matrix $\mathbf{W} = \text{diag}\{1 \ 20 \ 1\}$ was chosen to fade out collective input at around the minimum power required speed $V_{\text{CAS}} \approx 100$ kts (Ref. 4). The \mathbf{B} matrix from Eq. 2 is then multiplied by the control allocation matrix \mathbf{M} to get a square matrix that can be inverted for the $(\mathbf{CB})^{-1}$ block.

The control allocation matrix \mathbf{M} converts the longitudinal acceleration command \dot{V}_{cm} and vertical acceleration command \ddot{h}_{cm} into pitch attitude θ , symmetric main rotor collective δ_{col} , and pusher propeller collective δ_{prop} commands, and as such has units of deg/ft/sec². The pitch attitude θ , symmetric main rotor collective δ_{col} , and pusher propeller collective δ_{prop} commands generated by the control allocation block are perturbation values from the trim condition at which the control derivative matrix \mathbf{B} is determined (Ref. 24). Therefore, airspeed scheduled trim values of pitch attitude θ , symmetric main rotor collective δ_{col} , and pusher propeller collective δ_{prop} commands are summed with the perturbation values, downstream of the control allocation block.

Figure 3 shows the control allocation matrix \mathbf{M} as a function of airspeed V for the coaxial-pusher. As expected, in hover, \dot{V}_{cm} is allocated primarily to pitch attitude θ (similar to a typical helicopter) and some to pusher propeller collective δ_{prop} . As airspeed increases, \dot{V}_{cm} is allocated

less to pitch attitude and more to pusher propeller (similar to a typical fixed-wing aircraft). In hover, \ddot{h}_{cm} is allocated to symmetric main rotor collective δ_{col} , and as airspeed increases to pitch attitude θ . Again, this behavior is similar to a helicopter at hover/low-speed and converts to airplane-like control strategy at high speed. Note that at high speeds it appears from the plots in Figure 3 that the \ddot{h}_{cm} allocations all go to zero, however, this is because smaller values of pitch attitude θ are required to generate the same climb rate as airspeed increases. The third column of plots in Figure 3 shows a zoomed in view of the \ddot{h}_{cm} allocations at high speed, which show that pitch attitude θ and pusher propeller collective δ_{prop} are used at high speed.

Tiltrotor Control Allocation In the case of the tiltrotor, the outer-loop longitudinal acceleration command \dot{V}_{cm} and vertical acceleration command \ddot{h}_{cm} were allocated to pitch attitude and symmetric main rotor collective commands only. The nacelles were scheduled with commanded acceleration instead of being used as a dynamic input for the outer loops to control, which was done to avoid excessive hub moments and over-driving the nacelle actuators.

Since the tiltrotor lower-order dynamic inversion system is square, the \mathbf{B} matrix can be inverted, and the $(\mathbf{CB})^{-1}$ block acts as the control allocation. Figure 4 shows the tiltrotor outer-loop control allocation as a function of airspeed and nacelle angle. The control allocation is similar to that for the coaxial-pusher with \dot{V}_{cm} primarily being allocated to pitch attitude θ at hover/low-speed and symmetric main rotor collective δ_{col} at high speed. Vertical acceleration command \ddot{h}_{cm} is primarily allocated to collective at hover/low-speed and pitch attitude at high speed. The third column of plots in Figure 4 shows a zoomed in view of the \ddot{h}_{cm} allocations at high speed.

As with the coaxial-pusher, the pitch attitude θ and symmetric main rotor collective δ_{col} commands are perturbation values from the trim condition at which the control derivative matrix \mathbf{B} is determined. Therefore, airspeed and nacelle scheduled trim values of pitch attitude θ and symmetric main rotor collective δ_{col} are summed with the perturbation values, downstream of the $(\mathbf{CB})^{-1}$ block.

Figure 5 shows the outer-loop tiltrotor nacelle command schedule. The figure shows the conversion corridor of the tiltrotor as well as the path through the corridor (combinations of airspeed and nacelle angle) that results in a pitch trim attitude of $\theta_0 = 0$ deg (dashed blue line in Figure 5). Three nacelle schedules are used based on the sign (positive, negative, or zero) of the acceleration command \dot{V}_{cm} from the airspeed loop command model. When no acceleration is commanded ($\dot{V}_{\text{cm}} = 0$, red line in Figure 5), the nacelle schedule follows the $\theta_0 = 0$ deg schedule from hover to $V_{\text{CAS}} = 140$ kts. At speeds between

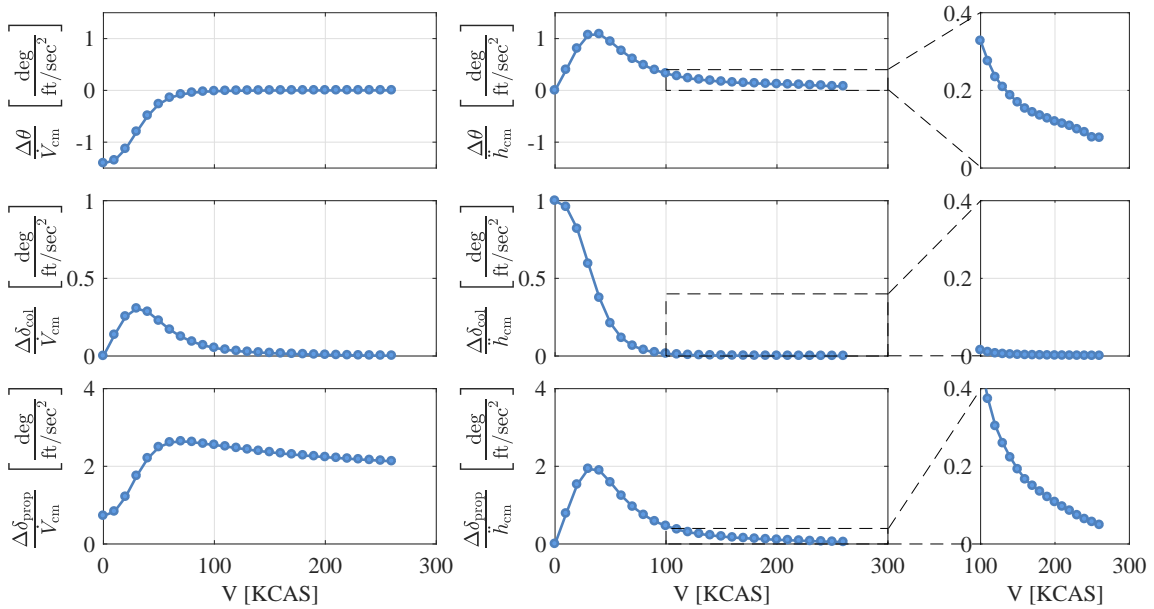


Fig. 3. Outer-loop control allocation (coaxial-pusher).

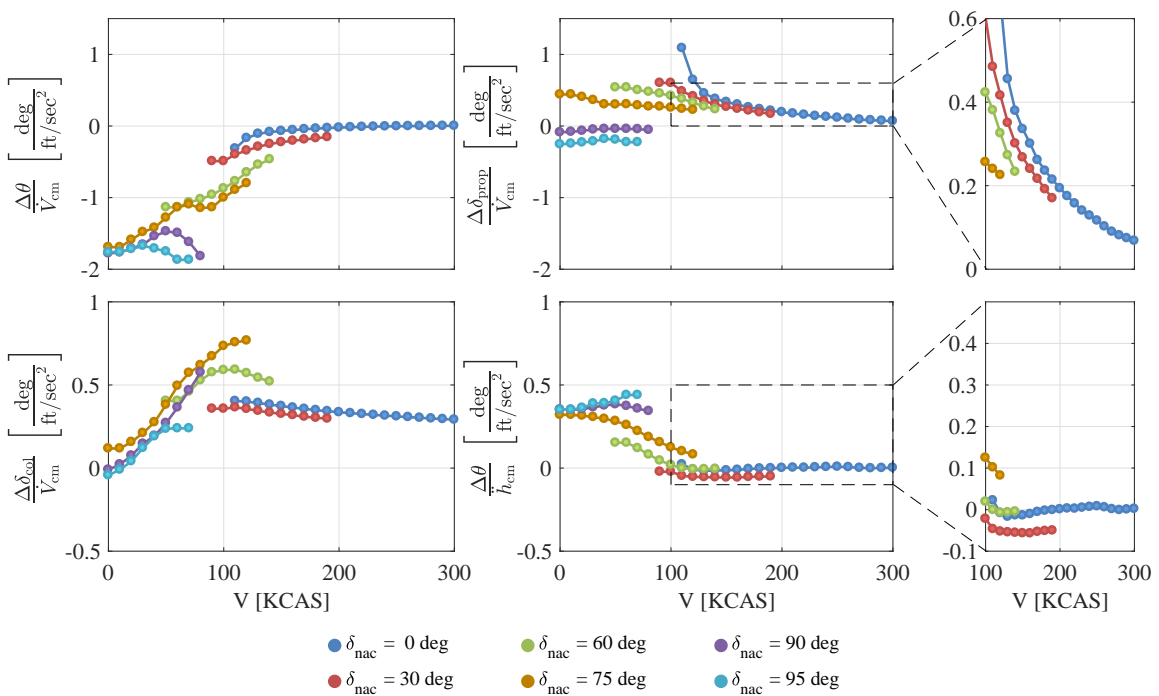


Fig. 4. Outer-loop control allocation (tiltrotor).

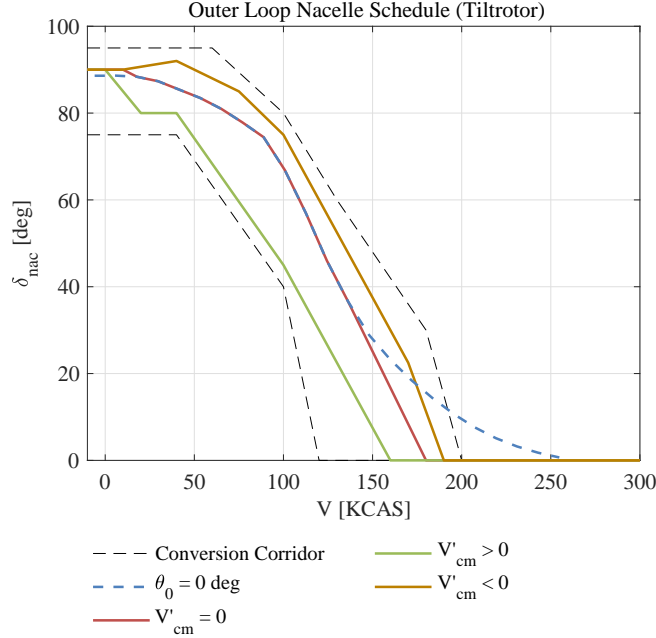


Fig. 5. Outer-loop nacelle schedule (tiltrotor).

$V_{CAS} = 140 - 180$ kts, the nacelle schedule linearly approaches $\delta_{nac} = 0$ deg, and above $V_{CAS} = 180$ kts the nacelle schedule is $\delta_{nac} = 0$ deg.

During acceleration ($\dot{V}_{cm} > 0$, green line in Figure 5), the nacelle schedule is closer to the bottom edge of the conversion corridor. This tracks the path through the corridor for fastest acceleration. In addition, this path has a trim pitch attitude that is $\theta_0 > 0$ deg. During acceleration, the outer loops command a negative pitch attitude as seen by the negative values in the first subplot in Figure 4. This ensures that the total pitch attitude which is the sum of trim and outer loop command will not be excessively nose-down.

Conversely, during deceleration ($\dot{V}_{cm} < 0$, orange line in Figure 5), the nacelle schedule is closer to the upper edge of the conversion corridor. As with the acceleration nacelle schedule, this ensures that the total pitch attitude will not be excessively nose-up.

Below $V_{CAS} = 10$ kts, all three nacelle schedules command $\delta_{nac} = 90$ deg.

4. Command Model

The command model in each axis sets the aircraft response characteristics to pilot inputs (i.e., response type, magnitude, and bandwidth). Table 1 lists the response type in the axes controlled by the outer loops as a function of airspeed. The lateral and directional axes response types were unchanged from those used for the inner-loop

control laws (Ref. 5). The collective stick δ_{col_s} generates an acceleration command response type using a first-order command model:

$$\frac{\dot{V}_{cm}}{\delta_{col_s}} = \frac{K_{col_{cm}}}{\tau_{col_{cm}}s + 1} \quad (4)$$

The command model gain was tuned based on the maximum acceleration and deceleration values at each airspeed. Maximum commanded acceleration $\dot{V}_{cm_{max+}}$ values are based on excess power P_{ex} :

$$K_{col_{cm}} = \dot{V}_{cm_{max+}} = \frac{P_{ex}}{(W/g)V} \quad (5)$$

In this case, the calculation of excess power as a function of airspeed was done offline, however, the control laws can easily be modified to dynamically change the command model gain $K_{col_{cm}}$ as a function of the actual excess power measured on board the aircraft (as done in Ref. 20). Maximum commanded deceleration values $\dot{V}_{cm_{max-}}$ are based on other aircraft limitation and were determined off-line as well.

Figures 6 and 7 show the airspeed command model parameters for the coaxial-pusher and tiltrotor, respectively. Note that for the stick gain $K_{col_{cm}}$ (top axis), two lines are shown: one for acceleration (positive values) and one for deceleration (negative values).

For the climb rate response, longitudinal stick commands climb rate \dot{h} for airspeeds between hover and $V_{CAS} = 40$

Table 1. Outer-Loop Control System Response Types

Speed Range [kts]	Longitudinal Cyclic	Thrust Control Lever
0–40	Vertical Rate Command / Height Hold	Ground Speed Acceleration Command / Speed Hold
40–300	Flight Path Rate Command / Attitude Hold	Airspeed Acceleration Command / Speed Hold

kts using a second-order command model:

$$\frac{\dot{h}_{cm}}{\delta_{lon_s}} = \frac{K_{lon_{cm}} \omega_{lon_{cm}}^2}{s + 2\zeta_{lon_{cm}} \omega_{lon_{cm}} s + \omega_{lon_{cm}}^2} \quad (6)$$

Above $V = 40$ kts, longitudinal stick commands flight path rate $\dot{\gamma}$ using a first order command model:

$$\frac{\dot{\gamma}_{cm}}{\delta_{lon_s}} = \frac{K_{lon_{cm}}}{\tau_{lon_{cm}} s + 1} \quad (7)$$

Flight path rate $\dot{\gamma}$ and angle γ are commanded and held, respectively, above $V = 40$ kts to aid in decelerating descending approaches. In these instances, if climb rate was held, the pilot would have to continuously adjust the commanded climb rate as airspeed varied to maintain the flight path vector.

Figures 8 and 9 show the flight path command model parameters for the coaxial-pusher and tiltrotor, respectively. Here, the stick gain $K_{lon_{cm}}$ was set to match the inner-loop $K_{lon_{cm}}$. The inner-loop $K_{lon_{cm}}$ commands 30 deg/sec of pitch rate between hover and $V_{CAS} = 110$ kts. Above $V_{CAS} = 110$ kts, the maximum pitch rate command is set to equal a normal acceleration of $n_z = 2.5$ g.

The flight path command model time constant, $\tau_{lon_{cm}}$ was chosen to have a flight path bandwidth of $\omega_{BW_\gamma} = 1.3$ rad/sec throughout the flight envelope.

A detailed study of what inceptor configuration pilots prefer to use with the outer-loop control laws is outside of the scope of this work. The outer-loop control laws described here were intended to be used with standard helicopter inceptors (sidestick, collective, and pedals). As such, a “Unified” control strategy (Refs. 25, 26) was used where the longitudinal cyclic sidestick commands rate of climb \dot{h} or flight path rate $\dot{\gamma}$ and the collective (or thrust control lever) commands longitudinal acceleration \dot{V} throughout the flight envelope. Although this control strategy works well for the F-35B and its mission (Ref. 26), since it is geared for and more intuitive in the high-speed flight regime, it is not necessarily the best solution for a helicopter and its specific mission. Since the research here is focused on transition and high-speed flight, this control strategy was adopted, however future

research should be focused on how to extend or blend this strategy with one more suited for the hover/low-speed flight regime.

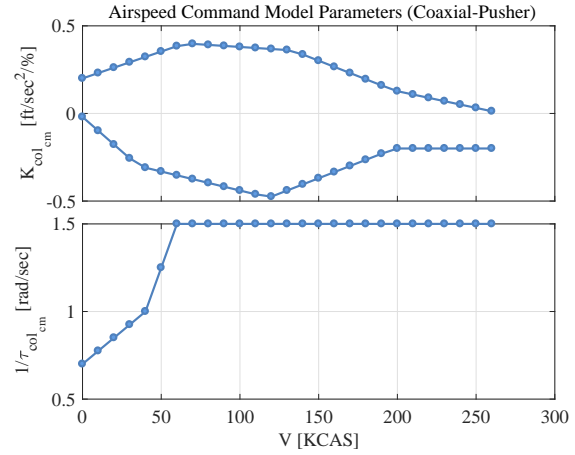


Fig. 6. Airspeed command model parameters (coaxial-pusher).

5. Command Delays

Command delays are used to synchronize the commanded and actual states in time, before determining the error used for feedback. The addition of command delays is typical in model following control laws (Ref. 11), and is done to account for higher-order dynamics and delays from the actuators, sensors, filters, and flight control computer processing time that are not accounted for by the inverse model. Accounting for this additional delay before comparing the commanded states with the actual states is useful to not overdrive the actuators. The addition of the command delays also reduces the amount of overshoot in the closed-loop end-to-end response with no added phase loss (Ref. 27).

6. Feedback

Proportional-plus-integral (PI) feedback is used in both channels of the outer loops, with the integral gain K_I constrained as a ratio of the proportional gain K_P . The ratio

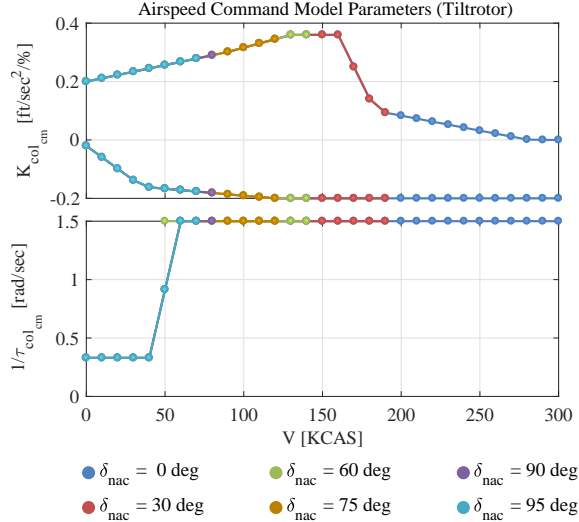


Fig. 7. Airspeed command model parameters (tiltrotor).

K_I/K_P sets the zero in the feedback, and is set to be:

$$\frac{K_I}{K_P} = \frac{\omega_c}{5} \quad (8)$$

where ω_c is the crossover frequency of the loop broken at the “Outer-Loop Stability Margin Break Point” in Figure 2. This ensures that the integral gain is effective, without overly degrading phase margin (Ref. 11).

The feedback gains were optimized to meet a comprehensive set of specifications, described in the next section, using a multi-objective optimization approach in CONDUIT[®] (Ref. 11).

SPECIFICATIONS

A common set of stability, handling-qualities, and performance specifications, shown in Table 2, was used to optimize both coaxial-pusher and tiltrotor outer-loop control laws using the CONDUIT[®] software tool (Ref. 11). The specifications were divided into two categories—Tier 1 and Tier 2 specifications (Ref. 11). Tier 1 specifications are key flight control and handling qualities requirements that drive the design optimization, and are guaranteed to be met for an optimized design. Tier 2 specifications are those which are evaluated only at the end of the optimization. These are typically alternate requirements that give insight into the design and generally overlap with Tier 1 specifications. Because they are not evaluated during the optimization, due to computational time considerations, they are not always met.

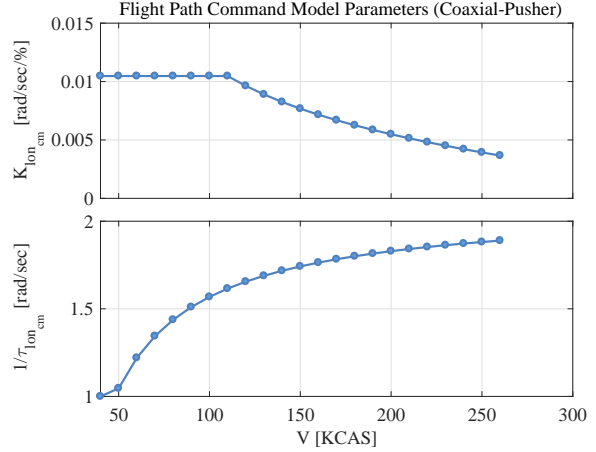


Fig. 8. Flight path command model parameters (coaxial-pusher).

Tier 1 Specifications

Twenty-three Tier 1 specifications were used for the outer-loop control laws divided into three categories which differentiate how they are handled during the control system optimizing (Ref. 11). The first category are the Hard Constraints, composed of the stability and stability margin requirements. During the first phase of the optimization, CONDUIT[®] ensures that these specifications are met, to ensure that a stable system is used to evaluate all subsequent specifications. Once all of the Hard Constraints are met, the CONDUIT[®] optimization ensures that the Soft Constraints are met, while not violating the already met Hard Constraints. The Soft Constraints are composed of the handling-qualities requirements. Finally, once all Hard and Soft Constraints are met, CONDUIT[®] works to minimize the Summed Objective requirements while not violating the Hard and Soft Constraints. The Summed Objectives are composed of actuator RMS and crossover frequency ω_c . Minimizing the Summed Objectives results in a *Pareto optimum* solution. This is the solution that has minimum over-design, and therefore makes the most economical use of the actuators and minimizes sensitivity to noise.

For the coaxial-pusher and tiltrotor outer-loop control laws, Tier 1 specifications were selected primarily from SAE AS94900 (Ref. 32) (stability margins) and ADS-33E (Ref. 33) (handling qualities requirements). Tier 1 specifications include absolute eigenvalue stability (CONDUIT[®] name EigLcG1), stability margins (StbMgG1), and Nichols margins (NicMgG1) requirements (Hard Constraints). These specifications ensure that the design is stable with sufficient stability margins for each control loop broken at the input to the control allocation matrix.

Table 2. Outer-Loop Control System Optimization Specifications

CONDUIT [®]					
	Spec Name	Description (Motivation)	Axis*	Speed Range [kts]	Source
Tier 1	<i>Hard Constraints (Stability Requirements)</i>				
	EigLcG1	Eignevalues in L.H.P. (Stability)	All	All	Generic
	StbMgG1	Gain and Phase Margin broken at outer loop break point (Stability)	V, γ	All	AS94900
	StbMgG1	Gain and Phase Margin broken at inner loop break point (Stability)	P	All	AS94900
	NicMgG1	Nichols Margins broken at outer loop break point (Stability)	V, γ	All	Ref. 28
	<i>Soft Constraints (Handling Qualities Requirements)</i>				
	ModFoG2	Command model following cost (HQ)	V, γ	All	Generic
	DstBwG1	Disturbance rejection bandwidth ≥ 0.75 rad/sec (Loads, Ride Quality)	V, γ	All	Ref. 29,30
	DstPkG1	Disturbance rejection peak ≤ 6 dB (Loads, Ride Quality)	V, γ	All	Ref. 29,30
	CrsMnG2	Minimum $\omega_c \geq 1.0$ rad/sec (Robustness)	V, γ	All	Generic
	EigDpG1	Eigenvalue Damping $\zeta \geq 0.5$ (HQ, Loads)	All	All	Generic
	OlpOpG1	Open Loop Onset Point, pilot input (PIO)	V, γ	All	Ref. 31
	OlpOpG1	Open Loop Onset Point, disturbance input (PIO)	V, γ	All	Ref. 31
	<i>Summed Objective (Performance Requirements)</i>				
CrsLnG1	Crossover Frequency (Act. Activity)	V, γ	All	Generic	
RmsAcG1	Actuator RMS (Act. Activity)	V, γ	All	Generic	
Tier 2	<i>Check Only</i>				
	BnwPiF1	Pitch attitude bandwidth and phase delay, forward flight (HQ)	P	60-300	ADS-33E
	FlpPiF1	Flight path response to pitch attitude (HQ)	γ	100-300	ADS-33E
	BnwPiL4	Bandwidth, phase delay (HQ)	P	60-300	MIL-STD-1797B
	BnwFpL1	Transient flight-path response (HQ)	P, γ	60-300	MIL-STD-1797B
	DrpPiL1	Pitch dropback (HQ)	P	60-300	MIL-STD-1797B
	CapPiL1	LOES Control Anticipation Parameters (HQ)	P	60-300	MIL-STD-1797B

* P = Pitch, V = Velocity loop, γ = flight path loop

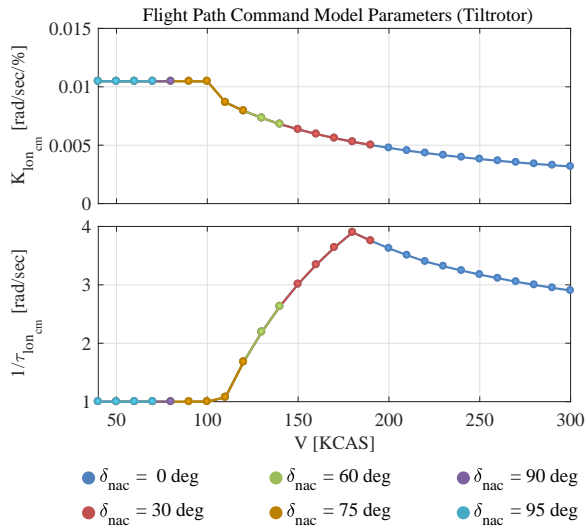


Fig. 9. Flight path command model parameters (tiltrotor).

Stability margin were evaluated for both airspeed and climb rate/flight path loops by breaking the loop at the outer-loop stability margin break point marked in Figure 2. In addition, stability margins of the inner pitch loop were evaluated with the outer loops closed by breaking the inner loop at the pitch command to the inner-loop control allocation matrix. Standard stability margin boundaries of gain margin $GM \geq 6$ dB and phase margin

$PM \geq 45$ deg (Ref. 32) are used throughout the flight envelope for the outer loops. In the case of the inner loop the standard stability margin boundaries were used for the coaxial-pusher throughout the flight envelope. For the tiltrotor, the inner-loop phase margin boundary was relaxed to $PM \geq 35$ deg for the mid-speed ($V_{CAS} = 50 - 100$ kts) speed range, since the standard phase margin requirement could not be met.

Soft Constraints include the model following cost specification (ModFoG2) which compares the closed-loop frequency response in each axis with the frequency response of the command model. A cost function J_{MF} is computed based on the weighted difference in the magnitude and phase of the responses, and a value of $J_{MF} \leq 50$ is enforced, ensuring good command model following in each axis (Ref. 11).

Disturbance rejection bandwidth (DRB, DstBwG1) and peak (DRP, DstPkG1) specifications (Refs. 29, 30) were enforced in each axis for the appropriate hold variable using boundaries of $DRB \geq 0.75$ rad/sec and $DRP \leq 6$ dB.

A minimum crossover frequency specification (CrsMnG2) was included for each axis. This specification ensures that the frequency response for each control loop broken at the input to the control allocation matrix has a crossover frequency above a specified value. The minimum crossover requirements are $\omega_c = 1.0$ rad/sec for both airspeed and climb rate/flight path channels. As shown in Eq. 8, the integral gains were

constrained to their respective proportional gains using the minimum crossover frequency specification value $\omega_c = 1.0$ rad/sec.

The Eigenvalue damping specification (EigDpG1) was used which evaluates the damping ratio of all closed-loop eigenvalues within a specified frequency range and compares them to the minimum required value.

The Open Loop Onset Point (OLOP, OlpOpG1) specification (Ref. 31) is included to evaluate the control law's susceptibility to Pilot Induced Oscillations (PIOs) and limit cycle oscillations that can result from actuator rate limiting. Linear analysis methods ignore the nonlinear effects of actuator position and rate limiting. However, the OLOP specification is based on frequency domain describing function concepts, and is useful to include in the design process to avoid exceeding the actuator limits of the aircraft.

Tier 2 Specifications

Six Tier 2 specifications were used as “check only” and not enforced by the control system optimization. The ADS-33E pitch attitude piloted bandwidth specification (BnwPiF1) and flight path response to pitch attitude specification (FlpPiF1) were included for high-speed flight ($V_{CAS} > 100$ kts). The pitch attitude bandwidth specification is included in the Tier 2 because the response type for the outer loops is flight path rate. Therefore, the pilot does not control pitch attitude directly. However, it is still desirable to have Level 1 values of pitch attitude bandwidth in case the pilot does decide to close the loop around pitch attitude while in this mode. In addition, since pitch attitude is an actuator to control climb rate/flight path for the outer loops, it is desirable to have a sufficiently fast pitch response.

The flight path response to pitch attitude specification ensures that the flight path or vertical rate response does not lag the pitch attitude response by more than $\phi = 45$ deg at all frequencies below $\omega = 0.4$ rad/sec. The relationship between flight path and pitch attitude is given approximately by (Ref. 16):

$$\frac{\gamma}{\theta} = \frac{1}{T_{\theta_2}s + 1} \quad (9)$$

where $1/T_{\theta_2}$ is the high-frequency pitch rate transfer function numerator zero. This parameter is a function of the bare-airframe, and since it shows up as a zero in the aircraft dynamics, it cannot be affected by feedback (although it can be through control allocation). Since this requirement does not drive the optimization of the feedback gains it is included as a Tier 2 specification.

Tier 2 specifications from MIL-STD-1797B consist of the pitch attitude (BnwPiL4) and flight path (BnwFpL1)

bandwidth, pitch attitude dropback (DrpPiL1), and Control Anticipation Parameter (CAP, CapPiL1) specification.

OPTIMIZATION STRATEGY

The control law parameters are gain scheduled as a function of airspeed for the coaxial-pusher. Parameters were determined at 10 kt increments from hover to $V_{CAS} = 260$ kts, for a total of 27 design points. For the tiltrotor, control law parameters are gain scheduled as a function of airspeed (from hover to $V_{CAS} = 300$ kts) and nacelle angle. A total of 71 design points were used for the tiltrotor, which are also in increments of 10 kts and span the conversion corridor.

At each design point, the command model parameters (stick gains and break frequencies) were hand-tuned to meet the piloted bandwidth requirements. The feedback gains were optimized in CONDUIT[®] using a multi-objective optimization approach to meet all of the Hard, Soft, and Summed Objective constraints (Ref. 11) listed in Table 2

OPTIMIZATION RESULTS

Coaxial-Pusher

Figure 10 shows several of the specifications and the optimized design values for several airspeeds ranging from hover to $V_{CAS} = 240$ kts. The first two rows of subplots show Tier 1 specifications: Stability margin, eigenvalue damping, minimum crossover frequency, and DRB/DRP. These are met for all of the designs through the optimization process.

The last row of subplots in Figure 10 shows several of the Tier 2 specifications. The first subplot is the ADS-33E flight path response to pitch attitude specification, which is met for all of the designs. Recall that this specification is equal to the bare-airframe $1/T_{\theta_2}$ (inverse flight path-attitude lag) and is not affected by the feedback.

The last three specifications in the third row of subplots in Figure 10 are the Tier 2 MIL-STD-1797B flight path versus pitch attitude bandwidth, CAP, and pitch attitude dropback specification. The flight path command model was tuned to give a flight path bandwidth $\omega_{BW_\gamma} = 1.3$ rad/sec, which corresponds to the flight path bandwidth values on the specification.

Since a constant flight path bandwidth ω_{BW_γ} value is enforced for all of the designs, the resulting pitch attitude bandwidth ω_{BW_θ} and dropback characteristics are a function of the bare-airframe $1/T_{\theta_2}$. Higher values of $1/T_{\theta_2}$ correspond to a shorter flight path to pitch attitude time lag. Therefore, for the same flight path bandwidth frequency, higher values of $1/T_{\theta_2}$ result in designs

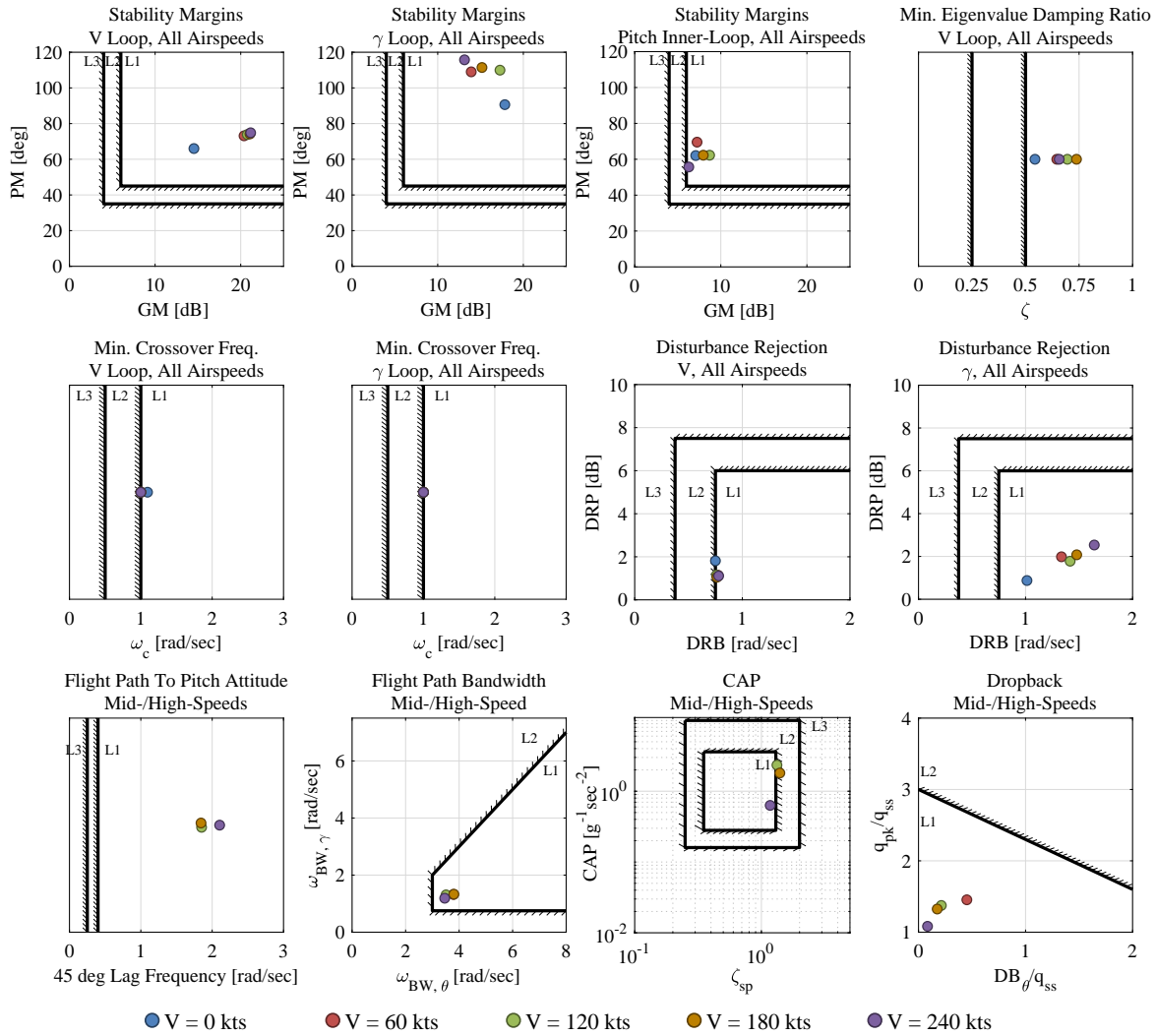


Fig. 10. Example control system design specification and optimized design results (coaxial-pusher, hover–240 kts).

with lower required values of pitch attitude bandwidth and lower value of pitch attitude dropback (as seen by comparing the designs at $V_{CAS} = 180$ and 240 kts in Figure 10).

Tiltrotor

Figure 11 shows several of the specifications and the optimized design values for several airspeeds ranging from hover to $V_{CAS} = 240$ kts. The first two rows of subplots show Tier 1 specifications: Stability margin, eigenvalue damping, minimum crossover frequency, and DRB/DRP. These are met for all of the designs though the optimization process.

The last row of subplots in Figure 11 shows several of the Tier 2 specifications. The first subplot is the ADS-33E flight path response to pitch attitude specification. The specification (equal to the bare-airframe $1/T_{\theta_z}$) is met for all of the designs, except slow speed airplane mode ($V_{CAS} = 120$ kts, $\delta_{nac} = 0$ deg), which is at the edge of the conversion corridor.

The second subplots in the last row in Figure 11 is the MIL-STD-1797B flight path versus pitch attitude bandwidth specification. All of the designs have a flight path bandwidth close to the design value of $\omega_{BW_\gamma} = 1.3$ rad/sec. The slower designs ($V_{CAS} = 60 - 120$ kts) have pitch attitude bandwidth in the Level 2 region of the specification.

The third subplots in the last row in Figure 11 is the MIL-STD-1797B Control Anticipation Parameter (CAP) specification. This requirement is met for all of the flight conditions except for $V_{CAS} = 60$ kts, $\delta_{nac} = 60$ deg which is also on the edge of the conversion corridor.

Finally, the last subplot in the last row in Figure 11 is the MIL-STD-1797B pitch attitude dropback specification. Since a constant flight path bandwidth ω_{BW_γ} value is enforced for all of the designs, the resulting dropback characteristics are a function of the bare-airframe $1/T_{\theta_z}$, with lower values of $1/T_{\theta_z}$ resulting in higher values of dropback.

HANDLING QUALITIES SIMULATION EXPERIMENTAL SETUP

Simulation Facility

The handling qualities experiment was conducted in the Pennsylvania State University (PSU) Flight Simulator facility, shown in Figure 12. The simulator consists of a raised Bell Helicopter BA609 simulation cab and a 5 m diameter spherical screen which provides 210 deg horizontal field of view and 50 deg vertical field of view. The simulator has motion capabilities, but they were not exercised for this experiment (i.e., experiment was carried out fixed-based).

Inceptors The inceptor configuration consisted of a passive sidestick [shown in Figure 13(b)] attached on the right-hand side by the pilot seat, standard active pedals, and a standard active collective stick [shown in Figure 13(a)] using pull-for-power logic. As discussed previously, the outer-loop control laws used the unified control inceptor approach. The collective stick is used to control longitudinal acceleration/deceleration throughout the flight envelope. In addition, pilots were also able to use the thumb hat switch on the collective [“1” in Figure 13(a)] to control acceleration and deceleration. Since this switch is discrete (commands 0 or 1), it commands maximum acceleration/deceleration when pressed.

The sidestick is used to command climb rate \dot{h} between hover and $V_{CAS} = 40$ kts and flight path rate $\dot{\gamma}$ above $V_{CAS} = 40$ kts. The button marked “4” in Figure 13(b) was used to set the commanded flight path angle or climb rate to zero, thus giving the pilots an easy way to null out their climb rate at high-speed, rather than hunting for $\gamma = 0$ with the sidestick. In addition, if the sidestick was in detent, and $|\gamma| < 1$ deg, the flight path rate command model automatically commanded $\gamma = 0$.

Buttons “2” and “3” on the sidestick were not active when the outer-loop control laws were engaged.

Nonlinear Simulation Model Validation

Before beginning handling qualities evaluations, implementation of the models in the simulator was validated. This was done by conducting both closed-loop and broken-loop automated frequency sweeps of the nonlinear simulation models. The frequency sweep simulation data were analyzed using CIFER[®] (Ref. 21) to extract the appropriate frequency responses and compare to those of the linear point model used in the control law development. Three responses were analyzed in each axis to validate the implementation of the feed-forward and feedback sections of the control laws: closed-loop piloted response, closed-loop disturbance response, and broken-loop response. Figure 14 shows an example validation result for the flight path broken-loop frequency responses of the coaxial-pusher at $V_{CAS} = 180$ kts. There is an excellent agreement between the nonlinear simulation and linear models, validating the implementation of the stitched model, gain schedule, and control laws in the simulation model. The remainder of the validation results show equally good agreement between the nonlinear simulation and linear models and are given in Ref. 17.

Handling Qualities Task Definitions

A subset of the MTEs used in the inner-loop handling qualities simulation experiment (Ref. 5) was used to test

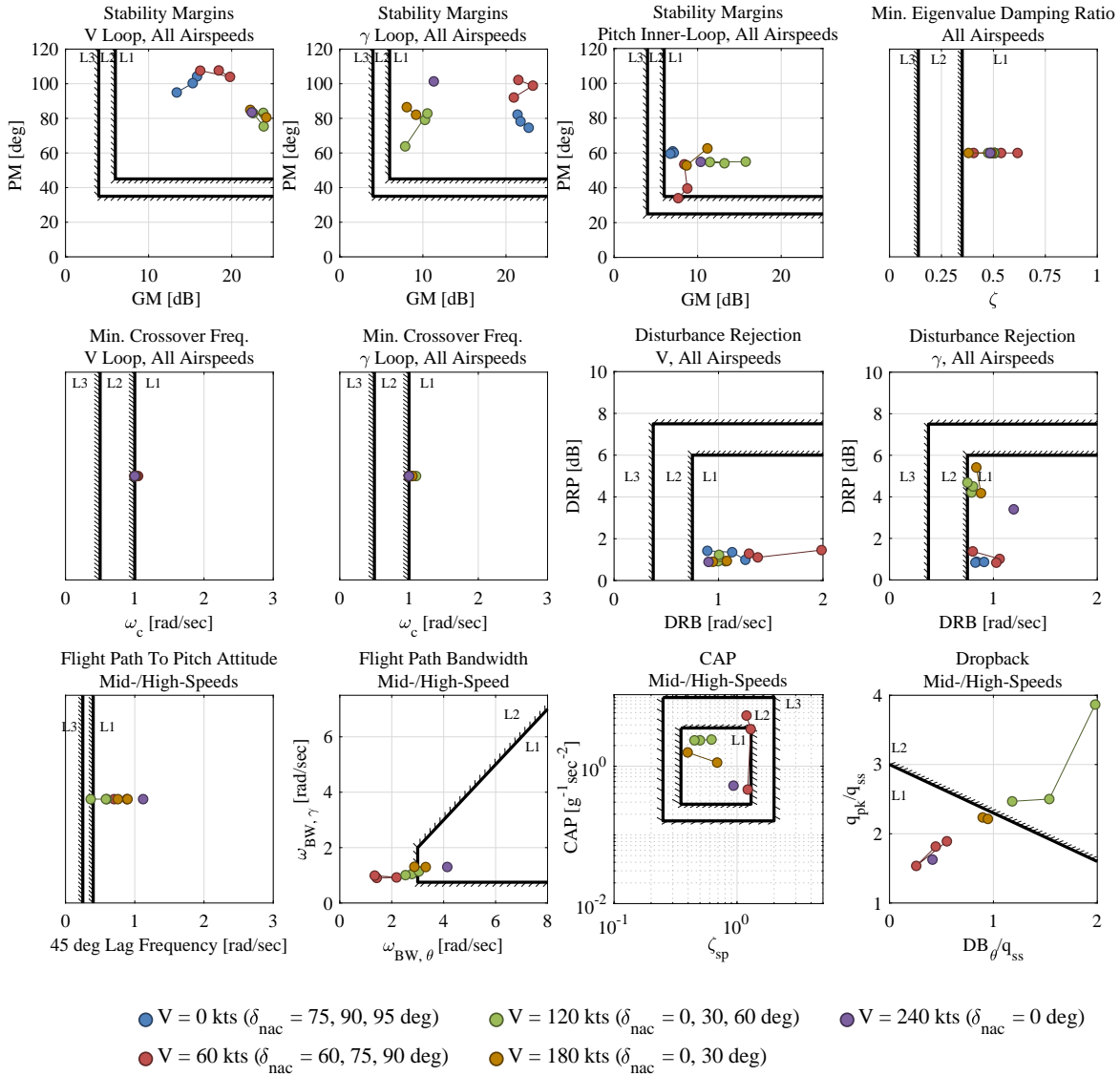


Fig. 11. Example control system design specification and optimized design results (tiltrotor, hover–240 kts).



Fig. 12. PSU Flight Simulator facility external view

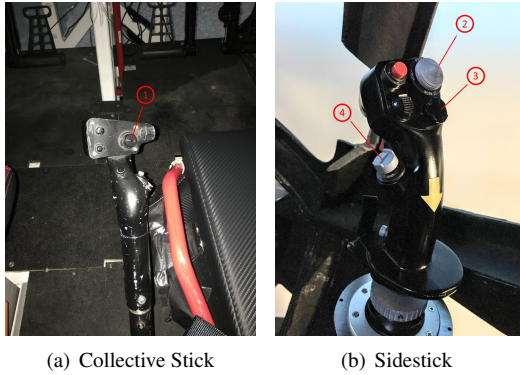


Fig. 13. PSU Flight Simulator facility inceptors.

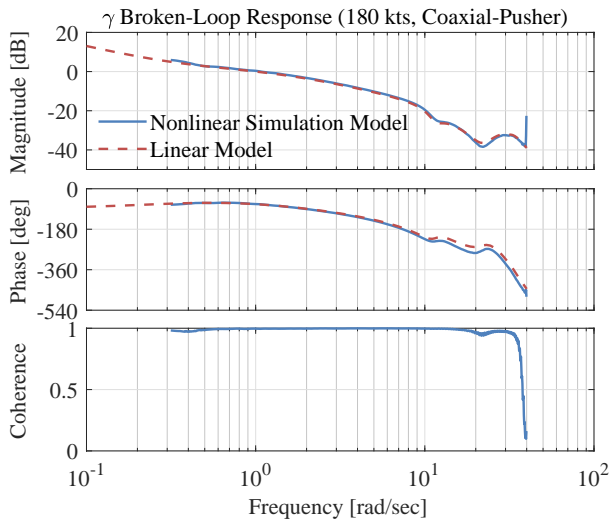


Fig. 14. Flight path broken-loop frequency response comparison (coaxial-pusher, 180 kts).

the outer loops. Since the outer loops only affect the longitudinal and heave axes, the following MTEs were tested were:

- *Pitch and Bank Attitude Capture and Hold* (Ref. 7): Precision, non-aggressive maneuvers flown using a special the display driven by a reference attitude signal composed of a series of step changes. The objectives of these tasks are to evaluate the ability to capture a desired attitude and identify maneuverability limitations, inceptor characteristics, cross coupling, and any PIO tendencies.
- *Pitch and Roll Sum-of-Sines Tracking* (Ref. 8): Precision tracking tasks flown using a special the display driven by a reference attitude signal composed of a sum of sines. The objectives of these tasks are to evaluate handling qualities in a tight, closed-loop tracking task, evaluate the feel system, control sensitivity, and cross coupling, and identify any bobble or PIO tendencies.
- *Break Turn* (Ref. 9): A non-precision, aggressive maneuver composed of a 90 deg heading change designed for evasive combat maneuvering. The task is meant to investigate any potential handling qualities issues or cliffs or pilot induced oscillation (PIO) tendencies resulting from aggressive roll-axis inputs.
- *High-Speed Acceleration/Deceleration* (Ref. 10): Evaluates up-and-away handling qualities in transitional flight for aircraft that experience significant configuration changes with airspeed. The maneuver is composed of two phases, a maximum performance level-flight acceleration, and a maximum performance level-flight deceleration, each of which has separate performance criteria and is rated separately.

For both aircraft, Pitch Attitude Capture and Hold, Pitch Sum-of-Sines Tracking, and Break Turn MTEs were flown at an airspeed of $V_{CAS} = 180$ kts, while a speed range of $V_{CAS} = 50 - 220$ kts was used for the High-Speed Acceleration/Deceleration.

As an additional test of the benefits of the outer-loop control laws, a fifth task was added (Formation Flying) which was not a formally defined MTE. The task involved getting into formation with a KC-130 aircraft with a trailing refueling probe, as shown in Figure 15. The KC-130 was flying straight and level at $V_{CAS} = 180$ kts for this task (although some initial investigations had the KC-130 dynamics driven by a sum-of-sines signal). The aircraft being tested started 10 kts slower, 450 ft in back, 250 ft to the left, and 200 ft below the KC-130. A heads-up display (HUD) was used (as shown in Figure 16) as a reference for the pilot to determine the formation position, where the waterline symbol on the HUD was over the drogue (as

shown in Figure 16). Since this was not a formal MTE with defined desired and adequate standards, only comments were collected from the pilots for this task (with no HQRs taken).

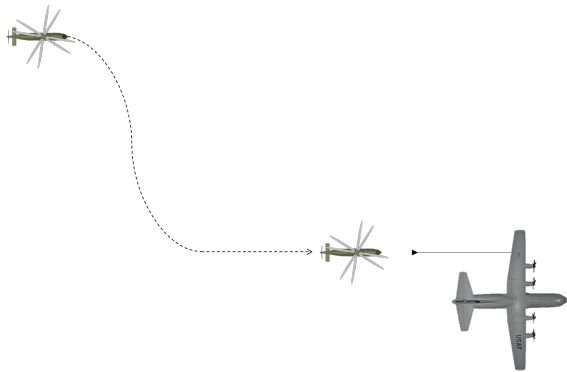


Fig. 15. Top-down view of formation task (roughly to scale).



Fig. 16. Pilot's view of formation position (note waterline symbol over refueling basket).

Pilot Questionnaire and Rating Scales

After several familiarization runs of each maneuver with each aircraft/control laws combination, pilots conducted two to three runs for record. Subsequently, they answered a questionnaire specifically tailored for this experiment and then used the Cooper-Harper Handling Qualities Rating Scale (Ref. 34) to provide a Handling Qualities Rating (HQR). For the Break Turn, and High-Speed Acceleration/Deceleration MTEs, pilot also used the Bedford Workload Scale (Ref. 35) to provide a Bedford Workload Rating (BWL). Finally, pilots were provided with a pilot induced oscillations (PIO) rating scale to use in case

they encountered any PIO, however none were encountered during testing.

Pilot Demographics

Two U.S. Army experimental test pilots (XPs) participated in the handling qualities assessment. Both had over 2,400 hours of total flight time and primarily flight experience in H-1, H-60, H-58, and H-47, but other aircraft have been evaluated. One of the two pilots also participated in the VMS simulation (Ref. 5) and was familiar with the tasks, aircraft models, and inner-loop control systems. The other pilot had experience flying the high-speed MTEs on a UH-60M Black Hawk (Ref. 6) and so was familiar with the tasks. He also had simulator tiltrotor experience.

COAXIAL-PUSHER HANDLING QUALITIES RESULTS

Figure 17 shows the Handling Qualities Ratings (HQRs) collected for the coaxial-pusher aircraft for the tasks flow in the PSU simulator. Results are shown for the inner-loop control laws (red squares) and outer-loop control laws (green triangles). In addition, the relevant results from the VMS simulation (Ref. 5) are shown for comparison (blue circles). The error bars represent average, maximum, and minimum ratings collected.

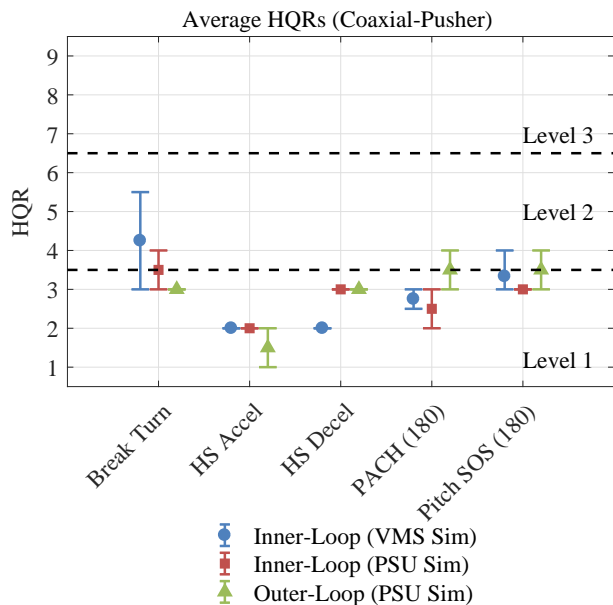


Fig. 17. Handling qualities rating summary (coaxial-pusher).

Average HQRs for the inner-loop control laws from the VMS experiment and PSU simulator experiment are within 1 HQR for all of the tasks, suggesting that the PSU simulator provided sufficient fidelity for conducting high-speed handling qualities evaluations. Therefore, the following sections will discuss the results from the PSU simulator experiment for each MTE in more detail.

Comparing the PSU simulator results for the inner- and outer-loop control laws, the outer-loop control laws improve the Break Turn ratings from borderline Level 1/Level 2 to Level 1. In addition, a half HQR point improvement is seen for the High-Speed Acceleration task, while the ratings for the High-Speed Deceleration are the same between the inner and outer loops. For both the Pitch Sum-of-Sines Tracking and Pitch Attitude Capture and Hold MTEs, the results for the outer loops are borderline Level 1/Level 2 while the result for the inner loop are Level 1.

Break Turn

Figure 18(a) shows the Break Turn MTE performance of the coaxial-pusher inner-loop control laws for all data runs for both pilots plotted against the desired and adequate bounds. Both pilots were able to meet desired performance, although both also had one record run with the time to complete beyond desired (i.e., adequate performance).

Figure 18(b) shows the Break Turn MTE performance of the coaxial-pusher outer-loop control laws for all data runs for both pilots. With the outer-loops engaged, times to complete for both pilots were shorter. In addition, there was less variability in airspeed V and altitude h during the maneuver, and the bank angle ϕ traces were qualitatively smoother.

Pilot A rated the Break Turn with the inner-loop control laws an HQR 3 and a Bedford Workload Rating (BWL) 4. For the outer-loop control laws, Pilot A rated the Break Turn MTE an HQR 3 and BWL 3. He commented that in the roll axes, there was no change between the inner- and outer-loop control laws (as expected since the roll axis is identical between the two sets of control laws). Furthermore, although he was consistently able to make desired performance with both control laws, there was “increased workload” with the inner loop, while it was “very easy” with the outer loop (as reflected in the BWL difference).

Pilot A noted that when flying the task with the inner-loop control laws, he had to worry about airspeed and altitude in addition to the roll attitude/heading task. With the outer-loop control laws, Pilot A commented that “airspeed maintenance was not required at all” and that the

control laws do a “good job of holding altitude.” He commented that his inputs were almost purely on the lateral stick, with several small pressure/counter-pressure inputs on the longitudinal stick to take out occasional altitude deviations. Pilot A commented that he rated the task an HQR 3 with the outer-loops because the most critical phase of the maneuver, which was targeting the desired heading and not overshooting bank angle on the roll out was similar to with the inner-loop control laws.

Pilot B rated the Break Turn an HQR 4 and a BWL 4 for the inner-loop control laws and an HQR 3 and BWL 4 for the outer-loop control laws. He commented that with the inner-loop control laws, the most challenging part of the maneuver was altitude control (which resulted in the HQR 4 rating), as well as not overshooting bank angle on the heading capture at the end of the maneuver. With the outer-loop control laws, Pilot B was able to be more aggressive and get shorter times to complete.

Overall, the results demonstrate the excellent airspeed and altitude hold performance of the outer-loop control laws. In addition, the pilot ratings show an improvement from borderline Level 1/Level 2 handling qualities with the inner-loop control laws to Level 1 handling qualities with the outer loop control laws. An average half-point reduction was also seen in the Bedford Workload Rating.

High-Speed Acceleration/Deceleration

Figure 19(a) shows the High-Speed Acceleration MTE performance of the coaxial-pusher inner-loop control laws for all data runs for both pilots plotted against the desired and adequate bounds. Both pilots were able to meet desired performance.

Figure 19(b) shows the High-Speed Acceleration MTE performance of the coaxial-pusher outer-loop control laws for all data runs for both pilots. Both pilots were also able to meet desired performance with the outer-loops engaged, and do so with faster times to complete the maneuver. This is because the outer-loop control system supplements the pusher propeller commands with pitch attitude θ to accelerate at lower speeds, as seen by comparing the last subplot in Figures 19(a) and (b).

Pilot A rated the High-Speed Acceleration MTE with the coaxial-pusher inner-loop control laws an HQR 2 (note, since this is a low-workload task, Bedford Workload Ratings were not collected). Pilot A commented that it was “effortless to meet desired [performance]” for this task. He did not have to make any longitudinal inputs to stay within the ± 100 ft altitude tolerance bounds, but noted that he could “because there [was] nothing else to do.”

Pilot A also rated the High-Speed Acceleration MTE with the coaxial-pusher outer-loop control laws an HQR 2. He noted again that it was easy to meet desired performance,

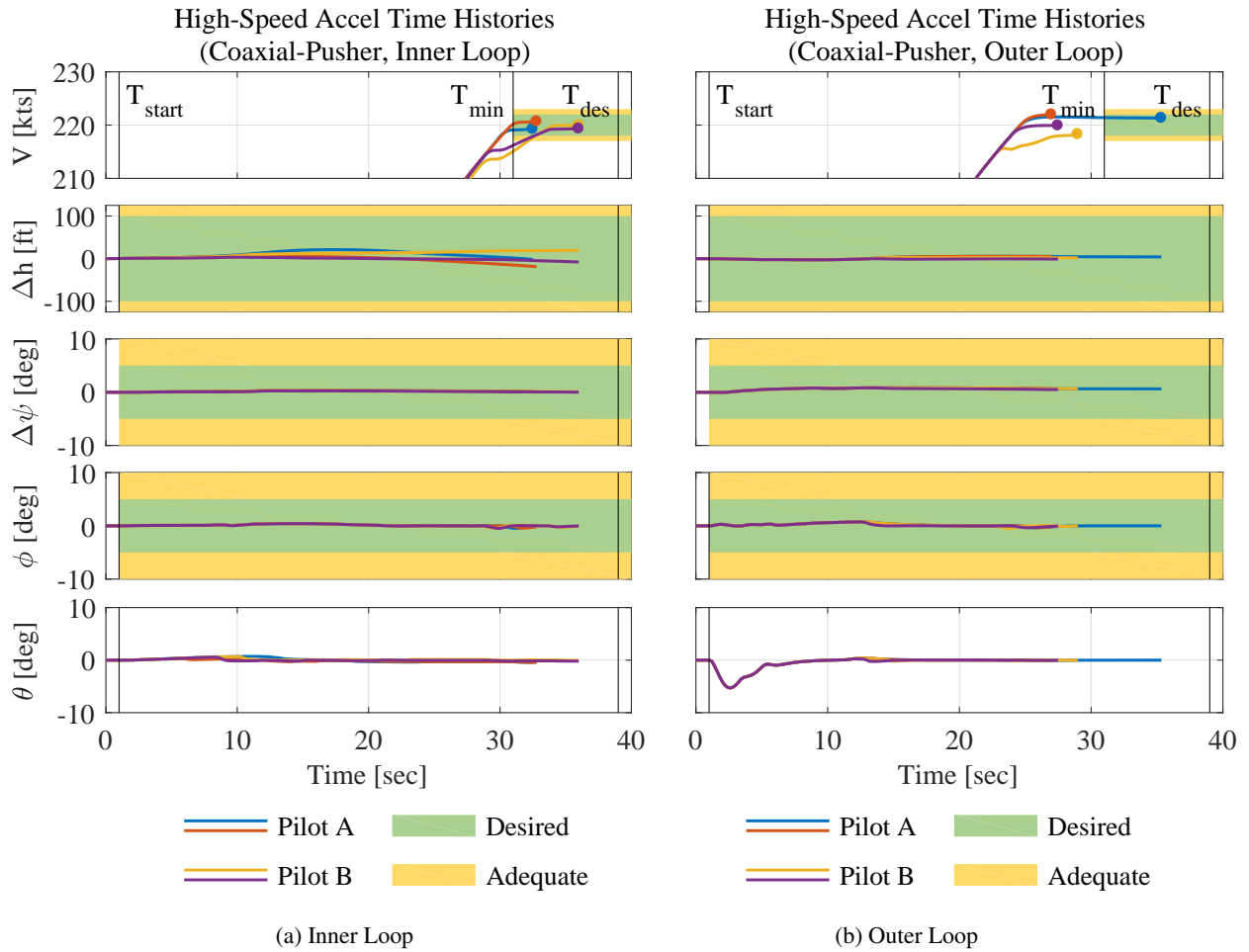


Fig. 19. High-Speed Acceleration task performance for (a) inner-loop control laws and (b) outer-loop control laws (coaxial-pusher, 180 kts).

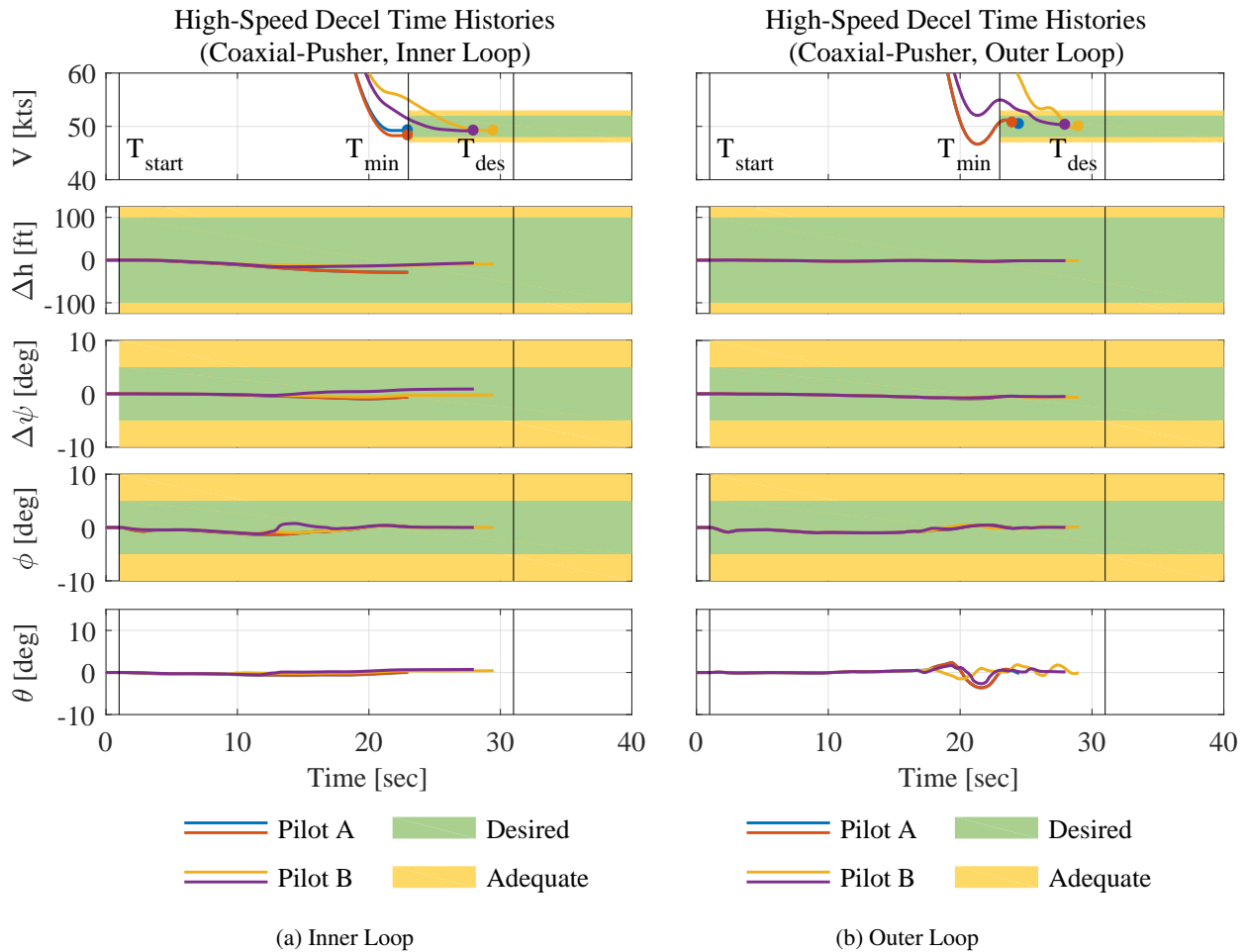


Fig. 20. High-Speed Deceleration task performance for (a) inner-loop control laws and (b) outer-loop control laws (coaxial-pusher, 180 kts).

but that it took slightly longer to null out the acceleration with the outer-loops than with the inner-loops.

Pilot B rated this task an HQR 2 with the inner-loop control laws and an HQR 1 with the outer-loop control laws. Pilot B similarly commented that it was “fairly easy to meet desired [performance]” with both inner- and outer-loop control laws.

Figure 20(a) shows the High-Speed Deceleration MTE performance of the coaxial-pusher inner-loop control laws for all data runs for both pilots plotted against the desired and adequate bounds. Both pilots were able to meet desired performance.

Figure 20(b) shows the High-Speed Deceleration MTE performance of the coaxial-pusher outer-loop control laws for all data runs for both pilots. Both pilots were also able to meet desired performance with the outer loops engaged, although tended to have more overshoot on the airspeed capture at the end of the maneuver.

Pilot A rated the High-Speed Deceleration MTE with the

coaxial-pusher inner-loop control laws an HQR 3. He performed the entire maneuver with two button presses, first the Set Zero Thrust button (Ref. 5), and then the Couple Thrust to Airspeed button (Ref. 5), and noted that no sidestick, pedals, or collective inputs were necessary. The critical phase of the task was timing nulling the deceleration with the Couple Thrust to Airspeed button press, which could be done precisely (within the ± 2 kts desired bounds).

With the outer-loop control laws, Pilot A similarly rated the High-Speed Deceleration MTE an HQR 3. Pilot A noted that he could be more precise using the collective for deceleration control rather than the thumb hat switch (since the thumb hat switch can only command maximum deceleration). Therefore, with the thumb hat switch he could be aggressive, but some guess work was required on the timing aspect which resulted in more over-/undershoots on speed captures.

Pilot B rated High-Speed Deceleration MTE an HQR 3

for both the inner- and outer-loop control laws. He noted that with the inner-loop control laws, there was an inability to accurately stop airspeed. However, he also noted that predictability of the outer-loop control laws was not as good on the deceleration as it was on the acceleration.

Overall, the coaxial-pusher inner-loop control laws with direct control of the pusher propeller thrust, provide Level 1 handling qualities for the High-Speed Acceleration/Deceleration tasks. In this case, the outer-loop control laws provided the same handling qualities Level as the inner-loop control laws.

Pitch Angle Capture and Hold

Figure 21 shows two example record runs for the Pitch Angle Capture and Hold MTE, one with the inner-loop control law and one with the outer-loop control laws. The two runs shown are representative of the additional record runs. Pilots were able to meet desired performance with both inner- and outer-loop control laws.

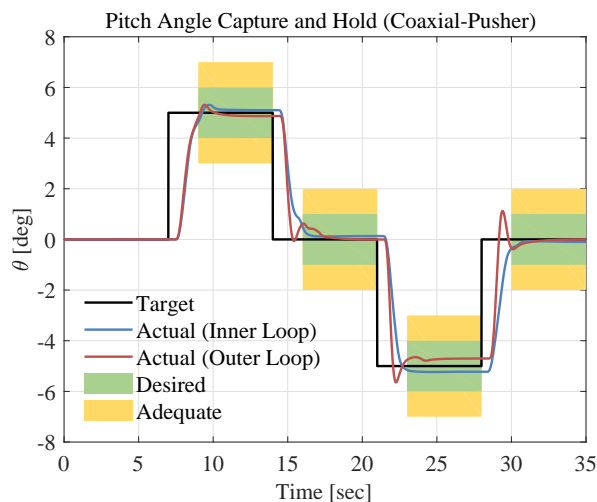


Fig. 21. Pitch Angle Capture and Hold example time history (coaxial-pusher, 180 kts).

Pilot A rated the Pitch Angle Capture and Hold MTE for the coaxial-pusher inner-loop control laws an HQR 2, and noted that he could be aggressive and that precision was not a problem. With the outer-loop control laws, Pilot A rated the Pitch Angle Capture and Hold MTE an HQR 4. He commented that the initial response was faster than he expected, and noted the pitch attitude dropback characteristic that was not present with the inner-loop control laws. He was able to compensate for the dropback, but referred to it as “annoying” which led to the Level 2 HQR.

Pilot B rated the Pitch Angle Capture and Hold MTE an HQR 3 for both the inner- and outer-loop control laws.

He noted that it was “easy to meet desired” with the inner-loop control laws and that the response was “very predictable.” With the outer-loop control laws, Pilot B noted that it required more control inputs to get same effect as the inner-loop control laws since he was compensating for the dropback characteristic.

Pitch Sum-of-Sines Tracking

Figure 22 shows the tracking performance for the Pitch Sum-of-Sines MTE for the coaxial-pusher. Only Pilot A flew this task for record, and was able to attain desired performance with both the inner- and outer-loop control laws.

Pilot A rated the inner-loop control laws an HQR 3 for this task and commented that the task was “not overly taxing.” He further noted that there was not much of a penalty for attempting to over-compensate in that he could stop the pitch rates generated and move back in the other direction quickly.

For the outer-loop control laws, Pilot A had similar task performance to the inner-loop control laws and also rated the task an HQR 3. However, for the outer loops he commented that although he was able to meet desired performance, it was “more difficult to be precise” and he was “working harder.” He further noted that the reversals were more difficult which led him to be less aggressive.

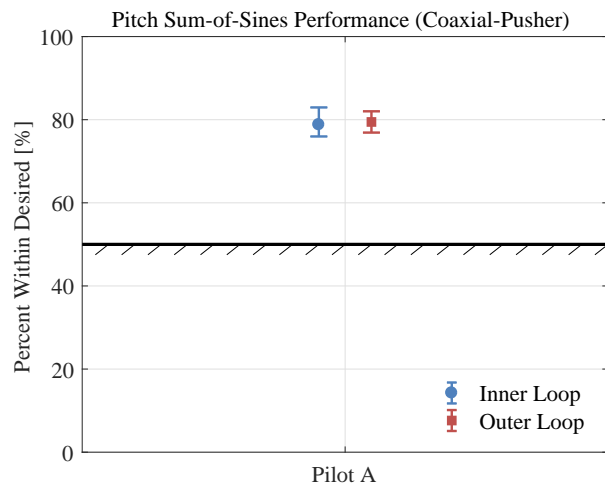


Fig. 22. Pitch Sum-of-Sines Tracking performance (coaxial-pusher, 180 kts).

Formation Flying

Figure 23 show the Formation Flying task time histories for two of Pilot B’s runs with the coaxial-pusher—one

with the inner-loop control laws and one with the outer-loop control laws. The figure shows the position error between the coaxial-pusher and the formation position, as well as the airspeed difference and climb rate traces for both control laws. Although Pilot B was able to move into the formation position equally well with both control laws, the climb rate trace in Figure 23 (bottom subplot) is less oscillatory with the outer-loop control laws.

Table 3 lists the lateral and longitudinal stick activity during this task. In the lateral axis, there was a 24% reduction in stick RMS for the outer-loop control laws as compared to the inner-loop control laws, while the cutoff frequency remained almost the same. In the longitudinal axis, where the outer-loop control laws are active, the stick RMS for the outer-loop control laws was 43% less than for the inner-loop control laws, while the cutoff frequency was about 25% less. These values demonstrate the lower workload of moving into the formation position with the outer-loop control laws than inner-loop control laws, and matched the pilot comments.

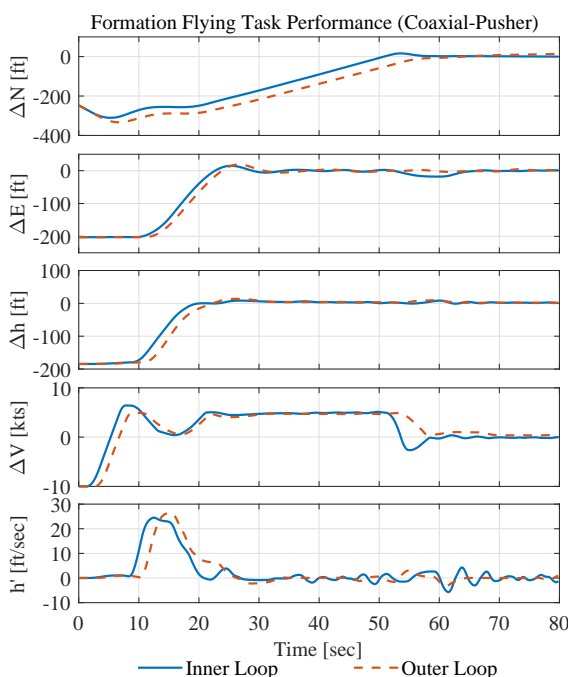


Fig. 23. Formation flying task performance (coaxial-pusher).

TILTROTOR HANDLING QUALITIES RESULTS

Figure 24 shows the Handling Qualities Ratings (HQRs) collected for the tiltrotor aircraft for the tasks flow in the PSU simulator. Results are shown for the inner-loop control laws (red squares) and outer-loop control laws (green

Table 3. Formation Flying Stick Activity (Coaxial-Pusher)

	Inner Loop	Outer Loop
<i>Lateral Stick</i>		
Cutoff Frequency ω_{co} [rad/sec]	2.44	2.29
Stick RMS [%]	3.71	2.82
<i>Longitudinal Stick</i>		
Cutoff Frequency ω_{co} [rad/sec]	1.81	1.36
Stick RMS [%]	4.53	2.56

triangles). In addition, the relevant results from the VMS simulation (Ref. 5) are shown for comparison (blue circles). The error bars represent average, maximum, and minimum ratings collected.

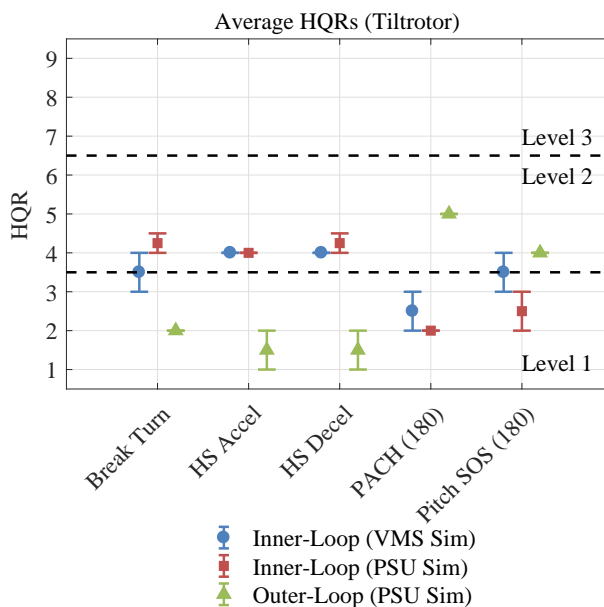


Fig. 24. Handling qualities rating summary (tiltrotor).

As with the coaxial-pusher results, average HQRs for the inner-loop control laws from the VMS experiment and PSU simulator experiment are within 1 HQR for all of the tasks, suggesting that the PSU simulator provided comparable fidelity to the VMS for conducting high-speed handling qualities evaluations.

Comparing the PSU simulator results for the inner- and outer-loop control laws, the outer-loop control laws improve the Break Turn ratings from Level 2 (average HQR 4.25) to Level 1 (average HQR 2). A significant improvement in handling qualities with the outer-loop control laws is also seen for the High-Speed Acceleration and Deceleration MTEs, with ratings going from Level 2 (av-

average HQR 4 for High-Speed Acceleration and average HQR 4.25 for High-Speed Deceleration) for the inner-loop control laws to Level 1 (average HQR 1.5 for both High-Speed Acceleration and Deceleration) for the outer-loop control laws.

In the case of the Pitch Attitude Capture and Hold and Pitch Sum-of-Sines Tracking MTEs, the results degraded for the outer-loop control laws, going from Level 1 ratings for the inner-loop control laws to Level 2 for the outer-loop control laws. The following sections will discuss the results for each MTE in more detail.

Break Turn

Figure 25(a) shows the Break Turn MTE performance of the tiltrotor inner-loop control laws for all data runs for both pilots plotted against the desired and adequate bounds. Pilot A was able to meet desired performance, while Pilot B met desired performance on all parameters except time to complete the maneuver (which was inside the adequate bounds).

Figure 25(b) shows the Break Turn MTE performance of the tiltrotor outer-loop control laws for all data runs for both pilots. With the outer-loops engaged, times to complete for both pilots were shorter and both pilots met desired performance on all of their runs. In addition, there was less variability in airspeed V and altitude h during the maneuver, and the bank angle ϕ traces were qualitatively smoother.

Pilot A rated the Break Turn MTE with the inner-loop control laws an HQR 4 and BWLR 7. He commented that he was “not guaranteed to make desired” when flying this task with the inner-loop control laws. He noted that he could be aggressive in roll and pitch, but that being precise was hard. Pilot A commented that the critical axis during this maneuver was pitch (trying to control vertical rate during the turn) even though the roll axis was also very active. In general, the bank angle was “a lot messier” with the inner-loop control laws because the focus was so much on pitch.

With the outer-loop control laws, Pilot A rated the Break Turn MTE an HQR 2 and a BWLR 3. He commented that the task was “much easier” and essentially became a single axis task where only rolling into and out of the turn had to be commanded by the pilot.

Pilot B rated the Break Turn MTE with the inner-loop control laws an HQR 4.5 (due to his times to complete being beyond the desired performance criteria). He commented that the aircraft response was predictable, but that when the aircraft was banked (during the steady portion of the turn), it was very pitch sensitive.

With the outer-loop control laws, Pilot B rated the Break Turn MTE with the tiltrotor an HQR 2. He commented

that it became “easy to meet desired [performance]” and that he was “monitoring the pitch axis rather than interacting with it.”

These results demonstrate the excellent airspeed and altitude hold capabilities of the outer-loop control laws.

High-Speed Acceleration/Deceleration

Figure 26(a) shows the High-Speed Acceleration MTE performance of the tiltrotor inner-loop control laws for all data runs for both pilots plotted against the desired and adequate bounds. Both pilots were able to meet desired performance.

Figure 26(b) shows the High-Speed Acceleration MTE performance of the tiltrotor outer-loop control laws for all data runs for both pilots. Both pilots were also able to meet desired performance with the outer-loops engaged, with significantly less variability in altitude and pitch attitude.

Pilot A rated the High-Speed Acceleration MTE with the tiltrotor inner-loop control laws an HQR 4 and BWLR 7. He commented that altitude was the most difficult variable to control during this task. This was because at the beginning of the task, the tiltrotor is controlled like a conventional helicopter, with pitch attitude being used to command acceleration [see negative pitch attitudes during first part of maneuver, Figure 26(a), bottom subplot]. Eventually, as airspeed increases and the wing becomes effective, pitch attitude has to be increased in order to have a positive angle of attack on the wing. Having to manage pitch attitude, collective, and nacelle angle during this task led to a high workload rating. Pilot A did note that near the end of the maneuver, in airplane mode, altitude was well behaved and he was only concentrating on using collective to manage airspeed.

Pilot A rated the High-Speed Acceleration MTE with the tiltrotor outer-loop control laws an HQR 2 and BWLR 3. He attempted the task using both the collective stick and thumb hat switch to control acceleration and was able to easily meet desired with both. Pilot A commented that precision was “great” and that the task did not require any control compensation. The only reason Pilot A rated the task an HQR 2 instead of HQR 1 was because he had to hold the thumb hat switch/collective up the entire run (as opposed to being able to set a final airspeed and having the outer-loop automatically go there).

Pilot B rated the High-Speed Acceleration MTE with the tiltrotor inner-loop control laws an HQR 4. He noted that to meet desired performance, he had to be very aggressive with power and nacelle and so the highest workload became managing altitude with the pitch axis. With the outer-loop control laws, Pilot B rated the task an HQR 1. He said the task was “easy” and only required holding the

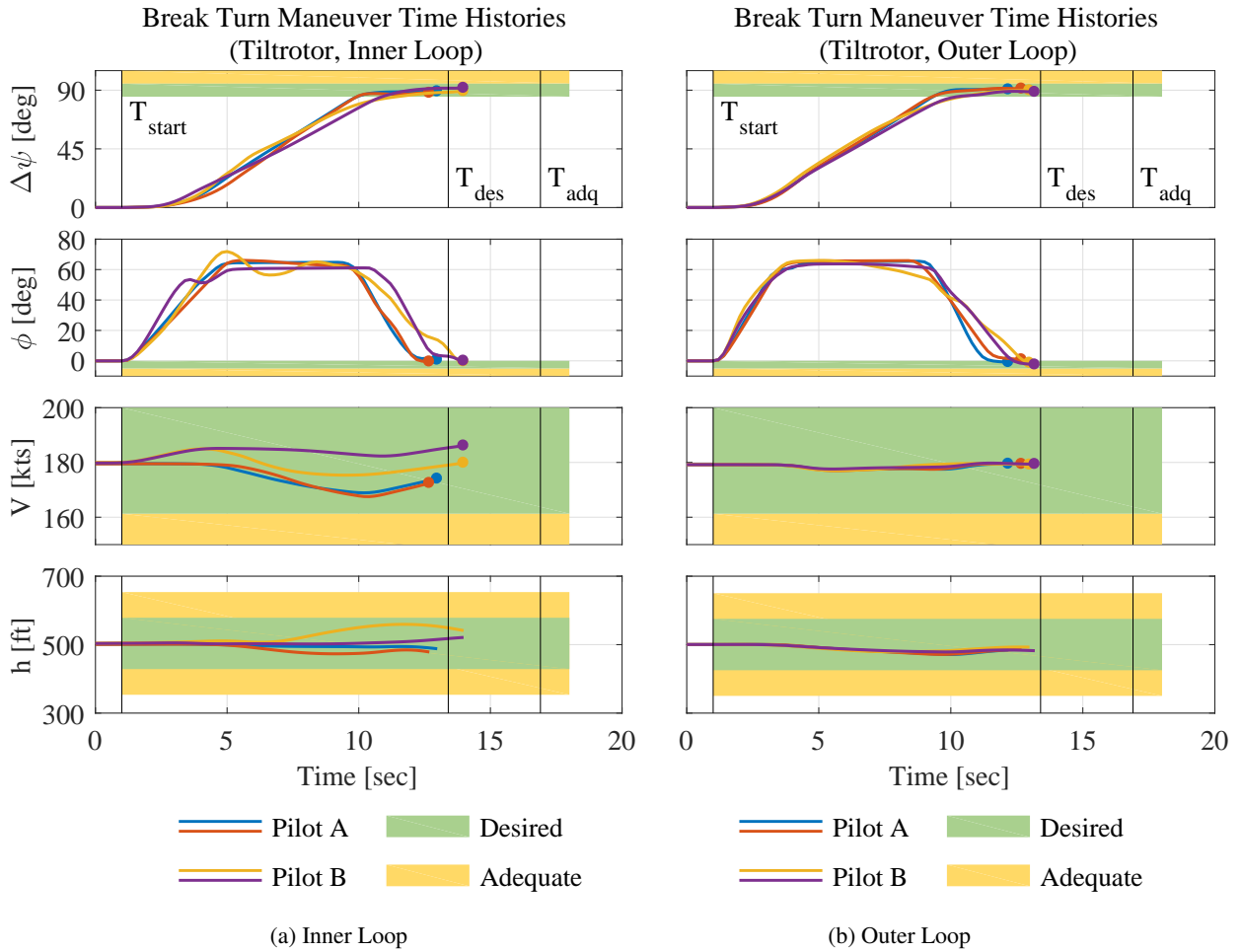


Fig. 25. Break Turn task performance for (a) inner-loop control laws and (b) outer-loop control laws (tiltrotor, 180 kts).

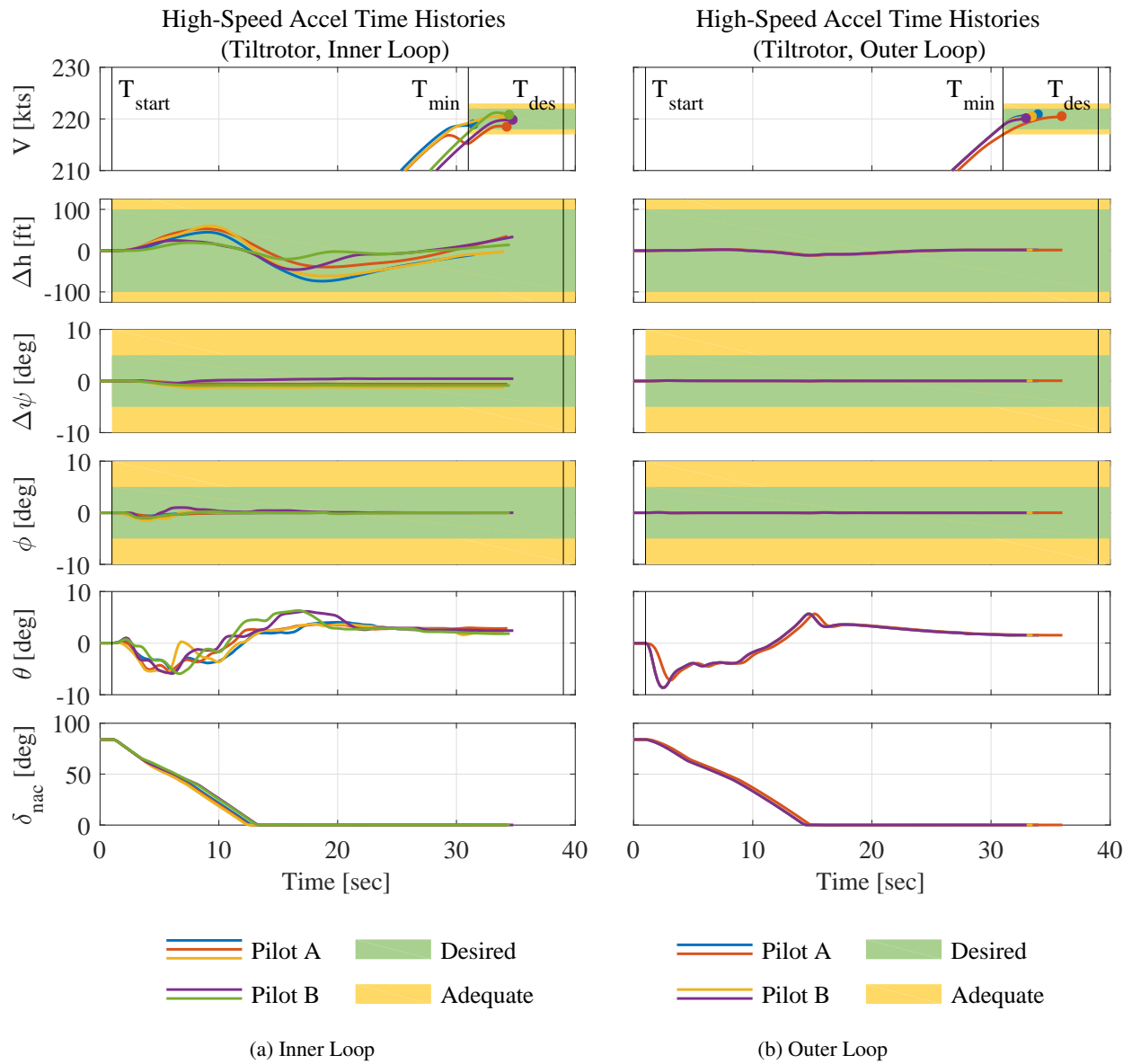


Fig. 26. High-Speed Acceleration task performance for (a) inner-loop control laws and (b) outer-loop control laws (right) (tiltrotor, 180 kts).

thumb hat switch down, with no control inputs required in pitch.

Figure 27(a) shows the High-Speed Deceleration MTE performance of the tiltrotor inner-loop control laws for all data runs for both pilots plotted against the desired and adequate bounds. Both pilots were able to meet desired performance. Pilot B had one run that was completed faster than the analytically determined minimum time to complete T_{\min} , due to the higher pitch attitude attained during the maneuver.

Figure 27(b) shows the High-Speed Deceleration MTE performance of the tiltrotor outer-loop control laws for all data runs for both pilots. Both pilots were able to meet desired performance with the outer-loops engaged, with significantly less variability in altitude and pitch attitude.

Pilot A rated the High-Speed Deceleration MTE with the tiltrotor inner-loop control laws an HQR 4 and BWLR 7. He commented that out of all of the maneuvers that he flew in this simulation experiment, this was the “busiest” one and that he could not individually isolate the controls. He had to use longitudinal stick, collective, and nacelle controls all at the same time. Although Pilot A noted that he was able to make desired performance and that there was “plenty of time” to complete the maneuver, he rated it an HQR 4 because of the difficult altitude maintenance.

With the outer-loop control laws, Pilot A rated the High-Speed Deceleration MTE an HQR 2 and BWLR 3. Pilot A attempted the deceleration with both collective and thumb hat switch and noted that it was easy to make desired performance with both. He did note that precision with the thumb switch was more difficult (because it only commands maximum deceleration) and timing the release took a few practice runs. However, the collective made it easier to be precise.

Pilot B rated the High-Speed Deceleration MTE with the tiltrotor inner-loop control laws an HQR 4.5, noting the high workload in the pitch axis to maintain altitude during the task. Pilot B rated the MTE an HQR 1 with the outer-loop control laws, and commented that altitude control was “very tight” and that the task became just a “single button press.”

Pitch Angle Capture and Hold

Figure 28 shows two example record runs for the Pitch Angle Capture and Hold MTE, one with the inner-loop control law and one with the outer-loop control laws. The two runs shown are representative of the additional record runs. Pilots were able to meet desired performance with the inner-loop control laws, but had some excursions into adequate performance with the outer-loop control laws, which drove the Level 2 HQRs for the outer loops.

Pilot A rated the inner-loop control laws an HQR 2 for the Pitch Angle Capture and Hold MTE. He commented that the response was “heavily/too damped” and that the aircraft felt like it had a lot of inertia. Pilot A noted that the response was predictable and easy to stop, although the slow initial acceleration caused him to lead his input to get a faster response.

For the outer-loop control laws, Pilot A rated the Pitch Angle Capture and Hold MTE an HQR 5. He commented that it was “hard to be precise” with this configuration since the magnitude of the overshoot was too big. This corresponds to the large value for pitch attitude dropback for the outer-loop control laws (Figure 11, last row, third subplot) as compared to the inner-loop control laws (Ref. 5).

Pilot B only tested the inner-loop control laws and gave an HQR 2. He commented that the speed of the responses was good, and that the response was “predictable” and “well behaved.”

These results suggest that the pitch attitude dropback value for the outer-loop control laws, which is in Level 1 at this airspeed, is too high and that the specification boundary may need to be reduced.

Pitch Sum-of-Sines Tracking

Figure 29 shows the performance for the Pitch Sum-of-Sines Tracking MTE for the tiltrotor. Both pilots were able to meet desired performance with both sets of control laws, although performance for the inner-loop control laws was significantly better for both pilots.

Pilot A rated the Pitch Sum-of-Sines Tracking MTE an HQR 2 for the inner-loop control laws. He commented that he had “no problem with precision,” was “not having to compensate,” and “definitely liked this one.” He also noted, though, that for the inner loops, although small pitch motions were “easy/nice,” large pitch motions were “hard.” This correlates well with Pilot A’s comments for the Pitch Attitude Capture and Hold task that the inner-loop control laws were too damped.

For the outer-loop control laws, Pilot A rated this task an HQR 4. He commented that he “could still get desired [performance],” but was required to “use a counter-move to get aircraft to stop.” The pitch attitude dropback was seen as uncommanded pitch motion by the pilot, which he referred to as an “annoying deficiency.”

Pilot B rated the Pitch Sum-of-Sines Tracking MTE an HQR 3 for the inner-loop control laws. He commented that he could “easily meet desired [performance]” and was “able to be aggressive.” Pilot B also noted that although the response was well damped, he “did not want quite as much [damping].”

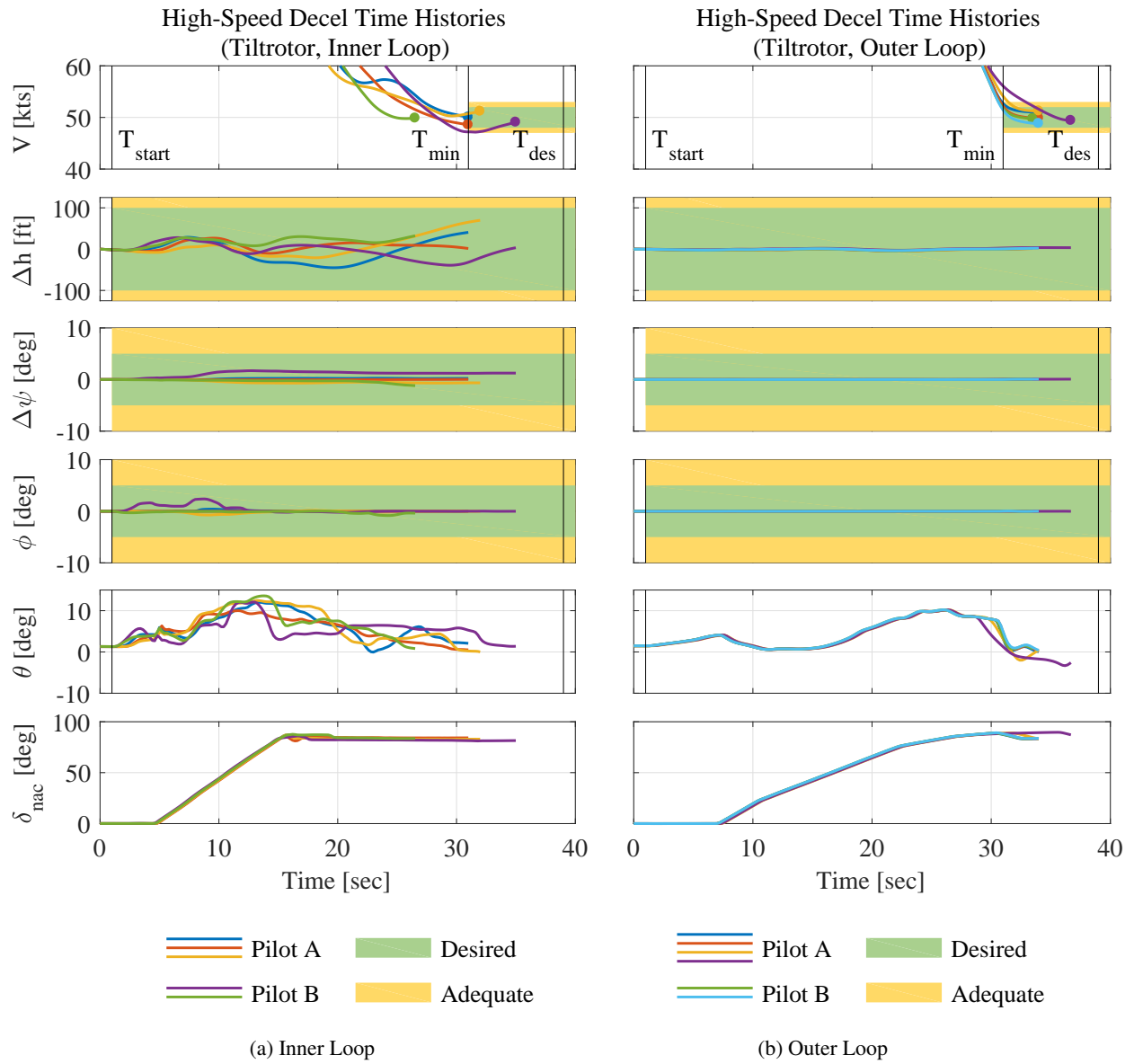


Fig. 27. High-Speed Deceleration task performance for (a) inner-loop control laws and (b) outer-loop control laws (tiltrotor, 180 kts).

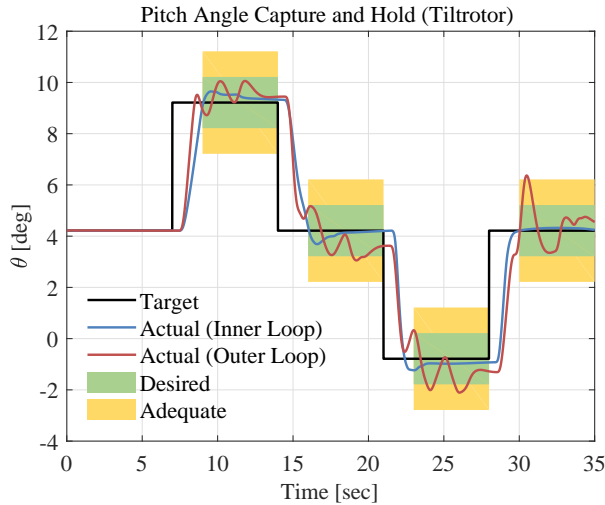


Fig. 28. Pitch Angle Capture and Hold example time histories (tiltrotor, 180 kts).

For the outer-loop control laws, Pilot B rated this task an HQR 4. He noted that the responsiveness of the outer-loop control laws was better, but with the penalty of overshoots. He also commented that although he was able to meet desired performance, his stress level went up with the outer-loop control laws as he was constantly making inputs and always fixing the over-/under-shoot.

Formation Flying

Figure 30 shows the Formation Flying task time histories for two of Pilot A’s runs with the tiltrotor—one with the inner-loop control laws and one with the outer-loop control laws. Pilot A was able to get into the formation position more quickly with the outer-loop control laws. Both airspeed and climb rate traces are much smoother and less oscillatory with the outer-loop control laws than with the inner-loop control laws. Pilot A commented that the task was “a lot easier” with the outer-loop control laws as compared to the inner-loop control laws.

Table 4 lists the lateral and longitudinal stick activity during this task. In both axes, the stick RMS was reduced for the outer-loop control laws and the cutoff frequency was higher. This is because with the outer-loop control laws, the pilot tended to make fewer, small inputs, both in terms of magnitude and duration. This correlates well with Pilot A’s comment that flying this task with the outer-loops was easier.

DISCUSSION

Overall, differences in Handling Qualities Ratings (both positive and negative) between the inner- and outer-loop

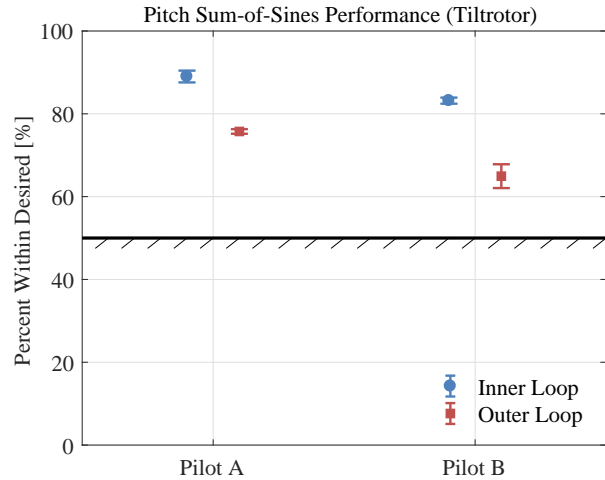


Fig. 29. Pitch Sum-of-Sines Tracking performance (tiltrotor, 180 kts).

Table 4. Formation Flying Stick Activity (Tiltrotor)

	Inner Loop	Outer Loop
<i>Lateral Stick</i>		
Cutoff Frequency ω_{co} [rad/sec]	1.17	3.75
Stick RMS [%]	3.64	2.58
<i>Longitudinal Stick</i>		
Cutoff Frequency ω_{co} [rad/sec]	0.815	3.05
Stick RMS [%]	3.51	2.56

control laws were larger for the tiltrotor than the coaxial-pusher for two main reasons. First, the coaxial-pusher has an independent thrust control (the pusher propeller) and the inner-loop control laws contain a collective trim map. This makes the High-Speed Acceleration/Deceleration MTEs with the inner-loop control laws a single, decoupled axis task with Level 1 HQRs, and the outer-loop control laws were not a significant improvement over this. The coaxial-pusher inner-loop control laws also received average borderline Level 1/Level 2 (HQR 3.5) ratings for the Break Turn MTE. The outer-loop control laws improved to a Level 1 rating of average HQR 3 for the Break Turn MTE.

However, in the case of the tiltrotor with inner-loop control laws, the High-Speed Acceleration/Deceleration MTEs were very dynamic and coupled tasks, where the pilot had to manage pitch attitude, collective, and nacelle angle manually. This resulted in high workload (BWL 7, which correlates to workload not tolerable for the task) and Level 2 HQRs for the inner-loop control laws. In contrast, the outer-loop control laws made the High-Speed Acceleration/Deceleration MTEs a single, decoupled axis task, where now the pilot only had to command accelera-

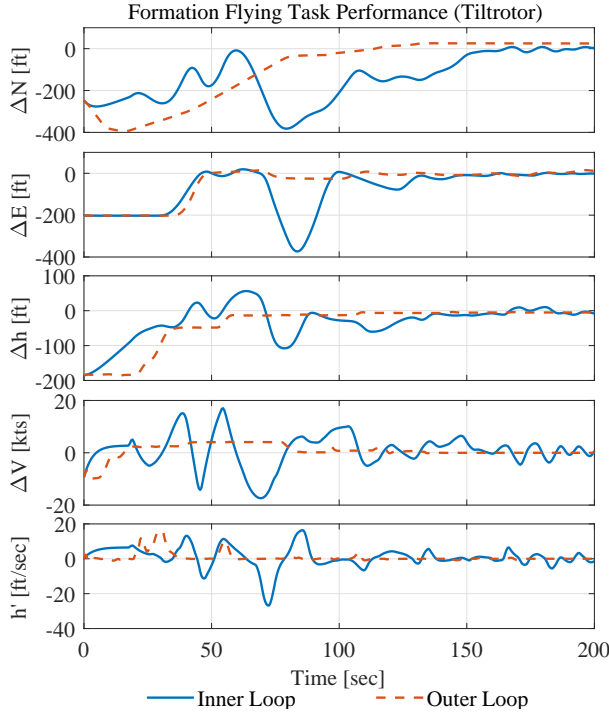


Fig. 30. Formation flying task performance (tiltrotor).

tion or deceleration directly, and the control system managed pitch attitude, collective, and nacelle angle. This resulted in a significant improvement in HQRs (average HQR 1.5) and reduction in workload (BWL 3, which correlates to workload satisfactory without reduction). In addition, the tiltrotor had a bigger improvement in HQRs for the Break Turn MTE, going from solid Level 2 handling qualities for the inner-loop control laws (average HQR 4.25) to solid Level 1 (average HQR 2).

The second reason for a larger difference in HQRs between the inner- and outer-loop control laws for the tiltrotor than the coaxial-pusher is the larger difference in pitch attitude dropback between the two control laws for the tiltrotor. This resulted in the outer-loop handling qualities of the tiltrotor degrading more than the coaxial-pusher for the Pitch Sum-of-Sines Tracking and Pitch Attitude Capture and Hold MTEs. In the case of the coaxial-pusher, there was a $\Delta\text{HQR} = 0.5$ degradation in handling qualities for the Pitch Sum-of-Sines Tracking MTE and a $\Delta\text{HQR} = 1.0$ degradation for the Pitch Attitude Capture and Hold MTEs with the outer-loop control laws. For the tiltrotor, with its large value of pitch attitude dropback for the outer-loop control laws, there was a $\Delta\text{HQR} = 1.5$ degradation in handling qualities for the Pitch Sum-of-Sines Tracking MTE and a $\Delta\text{HQR} = 3.0$ degradation for the Pitch Attitude Capture and Hold MTE with the outer-loop control laws.

The outer-loop control laws for both coaxial-pusher and tiltrotor have Level 1 pitch attitude dropback at the flight condition tested ($V_{\text{CAS}} = 180$ kts), however the pitch tracking tasks received borderline Level 1/Level 2 ratings for the coaxial-pusher and solid Level 2 ratings for the tiltrotor. In addition, most of the pilot comments about these configurations were about the dropback characteristics, confirming that dropback drove the HQRs. This suggests that the dropback requirement should be included as a Tier 1 specification in the control law design and enforced with a more stringent boundary (as discussed further in Ref. 17).

Overall, since the outer-loop control system improved handling qualities for some tasks (Break Turn and High-Speed Acceleration/Deceleration) while degraded handling qualities for other tasks (Pitch Attitude Capture and Hold and Pitch Sum-of-Sines Tracking), it should be implemented as a pilot selectable mode. The outer-loop control system is best suited for flight path control and gross maneuvering (e.g., getting into formation with a tanker aircraft), while the inner-loop control system is better suited for direct pitch attitude control (e.g., plugging the refueling probe into the refueling drogue).

CONCLUSIONS

This paper discussed the development and optimization of full-flight envelope outer-loop control systems for both coaxial-pusher and tiltrotor aircraft. A dynamic inversion control system architecture, based on a lower-order airspeed V and climb rate \dot{h} model, was used for both aircraft and was tuned to meet a common comprehensive set of stability, handling-qualities, and performance specifications. A piloted simulation experiment was conducted in the Pennsylvania State University (PSU) Flight Simulator facility to assess the handling qualities of the outer-loop control laws, with participation from two Army experimental test pilots. The results of the simulation experiment support the following conclusions:

1. A dynamic inversion architecture based on the identified two-state model worked well to control airspeed and climb rate/flight path throughout the full flight envelopes (hover-300 kts). Actual aircraft responses tracked the commanded responses well, with nearly no off-axis responses.
2. The multi-objective optimization method used to tune the feedback gains of the outer-loop dynamic inversion control system proved capable of determining designs which concurrently met a large number of frequency- and time-domain specifications while minimizing over-design (i.e., most economical use of actuators and noise sensitivity).

3. The outer-loop control laws significantly improved handling qualities and reduced pilot workload for the tiltrotor High-Speed Acceleration and Deceleration tasks by automatically managing nacelle tilt angle, symmetric rotor collective, and aircraft pitch attitude/angle of attack for the pilot. For the coaxial-pusher, with its direct thrust control, the outer-loop control laws had slightly better overall High-Speed Acceleration and Deceleration Handling Qualities Ratings than the inner-loop control laws.
4. The outer-loop control laws also improved the pilots' ability to get into formation with a simulated KC-130 aircraft, thus potentially improving handling qualities during an aerial refueling task.
5. A trade-off between the improved handling qualities and performance of the outer-loop control laws for the Break Turn, High-Speed Acceleration/Deceleration, and Formation Flying tasks was seen with the reduced performance and handling qualities during Pitch Sum-of-Sines Tracking and Attitude Capture and Hold tasks. This was due to the increased level of pitch attitude dropback of the outer-loop flight path rate command response type as compared to the inner-loop pitch rate command response type.
6. Overall, pilots preferred the Flight Path Rate-Command/Flight Path Angle-Hold response type of the outer-loops for gross maneuvering and flight path control, while for pitch tracking/pointing tasks they preferred a pitch RCAH response type. This suggests that the outer-loops should be implemented as a pilot selectable mode, which the pilot can engage based on the task they are performing (e.g., flight path vs. pitch attitude control).

ACKNOWLEDGMENTS

The authors would like to thank the pilots that participated in the handling qualities simulation assessment, LTC Dave Hnyda and Mr. John Wood, for providing their time, insight, and excellent comments.

REFERENCES

¹Graham, A., "FVL Update: Army, Navy and Marine Requirements Take Shape," *Vertiflite*, July/August 2019.

²Juhasz, O., Celi, R., Ivler, C. M., Tischler, M. B., and Berger, T., "Flight Dynamic Simulation Modeling of Large Flexible Tiltrotor Aircraft," American Helicopter Society 68th Annual Forum Proceedings, Fort Worth, TX, May 2012.

³Celi, R., "HeliUM 2 Flight Dynamic Simulation Model: Developments, Technical Concepts, and Applications," American Helicopter Society 71st Annual Forum, Virginia Beach, VA, May 2015.

⁴Berger, T., Juhasz, O., Lopez, M. J. S., Tischler, M. B., and Horn, J. F., "Modeling and Control of Lift Offset Coaxial and Tiltrotor Rotorcraft," *CEAS Aeronautical Journal*, Vol. 11, (1), January 2020, pp. 191–215.

⁵Berger, T., Blanken, C. L., Tischler, M. B., and Horn, J. F., "Flight Control Design and Simulation Handling Qualities Assessment of High-Speed Rotorcraft," Vertical Flight Society 75th Annual Forum Proceedings, Philadelphia, PA, May 2019.

⁶Berger, T., Ott, C. R., Cox, J. A., De Cecchis, P. M., and Wood, J. A., "Flight Test Assessment of the Break Turn and High-Speed Acceleration/Deceleration Mission Task Elements using a UH-60M Black Hawk," Vertical Flight Society 75th Annual Forum Proceedings, Philadelphia, PA, May 2019.

⁷Klyde, D. H., Pitoniak, S. P., Schulze, P. C., Ruckel, P., Rigsby, J., Xin, H., Fegely, C. E., Fell, W. C., Brewer, R., Conway, F., Mulato, R., Horn, J., Ott, C. R., and Blanken, C. L., "Piloted Simulation Evaluation of Attitude Capture and Hold MTEs for the Assessment of High-Speed Handling Qualities," American Helicopter Society 74th Annual Forum Proceedings, Phoenix, AZ, May 2018.

⁸Klyde, D. H., Pitoniak, S. P., Schulze, P. C., Ruckel, P., Rigsby, J., Xin, H., Fegely, C. E., Fell, W. C., Brewer, R., Conway, F., Mulato, R., Horn, J., Ott, C. R., and Blanken, C. L., "Piloted Simulation Evaluation of Tracking MTEs for the Assessment of High-Speed Handling Qualities," American Helicopter Society 74th Annual Forum Proceedings, Phoenix, AZ, May 2018.

⁹Xin, H., Fegely, C. E., Fell, W. C., Horn, J. F., Ruckel, P. D., Rigsby, J. M., Brewer, R. L., Conway, F. P., Mulato, R., Klyde, D. H., Pitoniak, S. P., Schulze, P. C., Ott, C. R., and Blanken, C. L., "Further Development and Piloted Simulation Evaluation of the Break Turn ADS-33 Mission Task Element," American Helicopter Society 74th Annual Forum Proceedings, Phoenix, AZ, May 2018.

¹⁰Brewer, R. L., Conway, F., Mulato, R., Xin, H., Fegely, C. E., Fell, W. C., Horn, J. F., Ruckel, P. D., Rigsby, J. M., Klyde, D. H., Pitoniak, S. P., Schulze, P. C., Ott, C. R., and Blanken, C. L., "Further Development and Evaluation of a New High-Speed Acceleration / Deceleration ADS-33 Mission Task Element," American Helicopter Society 74th Annual Forum Proceedings, Phoenix, AZ, May 2018.

- ¹¹Tischler, M. B., Berger, T., Ivler, C. M., Mansur, M. H., Cheung, K. K., and Soong, J. Y., *Practical Methods for Aircraft and Rotorcraft Flight Control Design: An Optimization-Based Approach*, AIAA, 2017.
- ¹²Cameron, N. and Padfield, G. D., "Tilt Rotor Pitch/Flight-Path Handling Qualities," American Helicopter Society 63rd Annual Forum Proceedings, Virginia Beach, VA, May 2007.
- ¹³Johnson, W., Moodie, A. M., and Yeo, H., "Design and Performance of Lift-Offset Rotorcraft for Short-Haul Missions," American Helicopter Society Future Vertical Lift Aircraft Design Conference Proceedings, San Francisco, CA, January 2012.
- ¹⁴Tobias, E. L. and Tischler, M. B., "A Model Stitching Architecture for Continuous Full Flight-Envelope Simulation of Fixed-Wing Aircraft and Rotorcraft from Discrete-Point Linear Models," U.S. Army AMRDEC Special Report RDMR-AF-16-01, April 2016.
- ¹⁵Stevens, B. L., Lewis, F. L., and Johnson, E. N., *Aircraft Control and Simulation: Dynamics, Controls Design, and Autonomous Systems, 3rd Ed.*, John Wiley & Sons, Inc., Hoboken, NJ, 2016.
- ¹⁶McRuer, D. T., Ashkenas, I. L., and Graham, D., *Aircraft Dynamics and Automatic Control*, Princeton University Press, Princeton, NJ, 1973.
- ¹⁷Berger, T., *Handling Qualities Requirements and Control Design for High-Speed Rotorcraft*, Ph.D. thesis, Pennsylvania State University, University Park, PA, December 2019.
- ¹⁸Horn, J. F., "Non-Linear Dynamic Inversion Control Design for Rotorcraft," *Aerospace*, Vol. 6, (3), 2019, pp. 38.
- ¹⁹Ozdemir, G. T., Horn, J. F., and Thorsen, A. T., "In-Flight Multi-Variable Optimization of Redundant Controls on a Compound Rotorcraft," AIAA Guidance, Navigation, and Control (GNC) Conference Proceedings, Boston, MA, August 2013.
- ²⁰Thorsen, A. T., *A Unified Control Methodology for a Compound Rotorcraft in Fundamental and Aerobatic Maneuvering Flight*, Ph.D. thesis, Pennsylvania State University, University Park, PA, December 2016.
- ²¹Tischler, M. B. and Remple, R. K., *Aircraft and Rotorcraft System Identification: Engineering Methods with Flight Test Examples, 2nd Ed.*, AIAA, Reston, VA, 2012.
- ²²Enns, D., "Control Allocation Approaches," AIAA Guidance, Navigation and Control Conference, Boston, MA, August 1998.
- ²³Ivler, C. M. and Juhasz, O., "Evaluation of Control Allocation Techniques for Medium Lift Tilt-Rotor," American Helicopter Society 71st Annual Forum Proceedings, Virginia Beach, VA, May 2015.
- ²⁴Durham, W., Bordignon, K. A., and Beck, R., *Aircraft Control Allocation*, John Wiley & Sons, Inc., Hoboken, NJ, 2017.
- ²⁵Rawnsley, B., Andrews, S., and D'Mello, G., "Future STOVL Flight Control: Development of Two-Inceptor Trimap Based Pitch Plane Control Law for the VAAC Research Aircraft," 1994 International Conference on Control Proceedings, Coventry, UK, March 1994.
- ²⁶Walker, G. P., Wurth, S., and Fuller, J., "F-35B Integrated Flight-Propulsion Control Development," 2013 International Powered Lift Conference Proceedings, Los Angeles, CA, August 2013.
- ²⁷Berger, T., Tischler, M. B., Hagerott, S. G., Gangsaas, D., and Saeed, N., "Longitudinal Control Law Design and Handling Qualities Optimization for a Business Jet Flight Control System," AIAA Atmospheric Flight Mechanics Conference Proceedings, Boston, MA, August 2012.
- ²⁸Magni, J. F., Bennani, S., and Terlouw, J., *Robust Flight Control: A Design Challenge*, Springer Verlag, Lecture Notes in Control and Information Sciences, Vol. 224, 1997.
- ²⁹Berger, T., Ivler, C. M., Berrios, M. G., Tischler, M. B., and Miller, D. G., "Disturbance Rejection Handling Qualities Criteria for Rotorcraft," American Helicopter Society 72nd Annual Forum Proceedings, West Palm Beach, FL, May 2016.
- ³⁰Blanken, C. L., Tischler, M. B., Lusardi, J. A., Berger, T., Ivler, C. M., and Lehmann, R., "Proposed Revisions to Aeronautical Design Standard-33E (ADS-33E-PRF) Towards ADS-33F-PRF," U.S. Army CCDC AvMC Special Report FCDD-AVM-19-01, September 2019.
- ³¹Duda, H., "Prediction of Pilot-in-the-Loop Oscillations due to Rate Saturation," *Journal of Guidance, Navigation, and Control*, Vol. 20, (3), May-June 1997.
- ³²Anon., "Aerospace - Flight Control Systems - Design, Installation and Test of Piloted Military Aircraft, General Specification For," SAE-AS94900, July 2007.
- ³³Anon., "Handling Qualities Requirements for Military Rotorcraft," Aeronautical Design Standard-33 (ADS-33E-PRF), US Army Aviation and Missile Command, March 2000.

³⁴Cooper, G. E. and Harper, J., R. P., "The Use of Pilot Rating in the Evaluation of Aircraft Handling Qualities," NASA TN D-5153, April 1969.

Scale for Assessing Pilot Workload in Flight: A Decade of Practical Use," Royal Aerospace Establishment, Technical Report TR 90019, March 1990.

³⁵Roscoe, A. H. and Ellis, G. A., "A Subjective Rating